

**Forschungszentrum Karlsruhe**

Technik und Umwelt

Wissenschaftliche Berichte

FZKA 6401

Performance Limits of a Helium-Cooled Divertor  
(Unconventional Design)

Final Report on Subtask PPA1.3.2  
of the  
Preparation of a Power Plant Conceptual Study  
on Plant Availability

K. Kleefeldt, S. Gordeev

Institut für Reaktorsicherheit  
Projekt Kernfusion

Forschungszentrum Karlsruhe GmbH, Karlsruhe  
2000

**Note:**

This work has been performed in the framework of the  
Nuclear Fusion Project of the Forschungszentrum Karlsruhe GmbH  
and is supported by the European Communities  
within the European Fusion Technology Programme

# Abstract

## Performance Limits of a Helium-Cooled Divertor (Unconventional Design)

In the frame of preparatory work for an European power plant conceptual study to be launched in 2000, the potential of different blanket and divertor cooling concepts has been assessed with view to their performance limits in a commercial reactor. As part of this activity the present work covers investigations related to the performance of a helium-cooled divertor, employing refractory materials as structure, able to extract high-grade heat for power conversion. Performance limits in terms of maximum achievable heat flux at divertor target plates are set mainly by materials temperature and stress constraints, but also by general design requirements like pumping power and tolerable deformation. In this context a high structure-to-coolant heat transfer is essential, which the porous media (PM) heat exchanger concept promises to provide effectively. Hence, the PM is the key design feature adopted in this study. Other basic elements of the assessment are assumptions on divertor configuration and operating conditions (dimensions, cooling scheme, power division to sub-components), material data base review for refractory materials involved, and a review of alternative heat transfer enhancement methods. The main part of the study covers the analysis methods and results of the proposed concept, which are grouped in overall divertor cooling parameters, thermal-hydraulics of target plate, and thermomechanical aspects of a single target plate cooling channel. Finally, the maximum tolerable heat flux is assessed based on limits set by temperature windows, thermal stresses and deformations. It is shown that heat fluxes of 5.5 to 6 MW/m<sup>2</sup> can be handled with helium-cooled concepts of unconventional design, given that the operating temperature in the only structural material deemed viable (molybdenum and tungsten alloys) must not fall below 600-700 °C for reasons of embrittlement. The potential for further improvements is judged to be marginal. Coolant parameters can be kept in an attractive range for power conversion.

## Zusammenfassung

### Belastungsgrenzen eines heliumgekühlten Divertors (neuer Bauart)

Im Rahmen von Voruntersuchungen für eine europäische Leistungsreaktorstudie, die im Jahre 2000 beginnen soll, wurden die Leistungsgrenzen verschiedener Blanket- und Divertorkonzepte für den Einsatz in kommerziellen Reaktoren untersucht. Als Teil davon werden in der vorliegenden Arbeit die Belastungsgrenzen eines heliumgekühlten Divertors aus temperaturbeständigem Material aufgezeigt, der die Nutzung der anfallenden Wärme für die Energieumwandlung ermöglichen soll. Die Belastungsgrenzen, gemessen an den zulässigen Wärmestromdichten an der Oberfläche der Divertorplatten, sind im wesentlichen bestimmt durch Grenzwerte für Temperatur und Spannung der verwendeten Werkstoffe, aber auch durch allgemeine Auslegungsanforderungen wie Gebläseleistung oder zulässige Verformungen der Bauteile. Ein guter Wärmeübergang zwischen Struktur und Kühlmittel ist hierbei unabdingbar. Dies lässt sich durch verschiedene Maßnahmen erreichen, unter anderem durch die Verwendung eines porösen Körpers (engl. porous media, PM) als wärmeübertragende Zwischenschicht, welcher hier als Hauptmerkmal bei der Auslegung zugrunde gelegt wurde. Weitere Grundannahmen betreffen den Aufbau und die Betriebsbedingungen des Divertors (Abmessungen, Kühlungsführung, Leistungsverteilung auf Komponenten), sowie die Datenbasis der in Frage kommenden Werkstoffe. Auch wurde eine Beurteilung anderer bekannter Methoden zur Verbesserung des Wärmeüberganges vorangestellt. Der Hauptteil der Studie befasst sich mit der Analyse des vorgeschlagenen Divertorkonzeptes unterteilt nach Ermittlung der Hauptparameter des Kühlsystems, thermohydraulische Auslegung der Kühlplatte und mechanisches Verhalten eines einzelnen Kühlkanals. Schließlich wird die zulässige Wärmestromdichte anhand von Temperatur-, Spannungs- und Verformungskriterien ermittelt. Es wird gezeigt, dass Wärmestromdichten von 5.5 bis 6 MW/m<sup>2</sup> von einem heliumgekühlten Divertor dieser Bauart aufgenommen werden können. Hierbei ist vorgegeben, dass die Betriebstemperatur der in Frage kommenden Werkstoffe (Molybdän- oder Wolframlegierungen) wegen Versprödung unter Bestrahlung nicht unter 600-700 °C liegen darf. Der Spielraum für weitere Optimierungen wird als gering eingeschätzt. Die Hauptparameter des Kühlsystems liegen in einem für die Leistungsumwandlung geeigneten Bereich.

# Table of Contents

<b>CHAPTER 1 - INTRODUCTION</b>	<b>1</b>
<b>CHAPTER 2 - OVERALL DIVERTOR DESIGN CONSIDERATIONS</b>	<b>3</b>
<b>2.1 Assumptions on divertor configuration and operating conditions</b>	<b>3</b>
2.1.1 Main dimensions	3
2.1.2 Assumed cooling scheme	3
2.1.3 Power to divertor and spatial distribution	4
<b>2.2 Materials involved</b>	<b>6</b>
2.2.1 General materials considerations	6
2.2.2 Material data	7
<b>2.3 Rationale for the design proposal</b>	<b>9</b>
2.3.1 Review of heat transfer enhancement methods	9
2.3.2 Selection of cooling method for target plates	12
2.3.3 Target plate design and operational window	13
<b>CHAPTER 3 - ANALYSIS OF PROPOSED CONCEPT</b>	<b>15</b>
<b>3.1 Type of analysis and methods used</b>	<b>15</b>
3.1.1 Outline of overall divertor cooling assessment	15
3.1.2 Outline of target plate thermal-hydraulics	16
3.1.3 Outline of thermomechanical analysis	17
<b>3.2 Analysis results</b>	<b>18</b>
3.2.1 Overall divertor cooling parameters	18
3.2.2 Thermal-hydraulics analysis of target plate	21
3.2.3 Thermomechanical analysis of target plate	24
<b>CHAPTER 4 - PERFORMANCE LIMITS AND OPEN ISSUES</b>	<b>27</b>
<b>4.1 Performance limits of proposed design</b>	<b>27</b>
4.1.1 Heat flux limits set by temperatures	28
4.1.2 Heat flux limits set by stresses	28
4.1.3 Heat flux limits set by deflections	28
4.1.4 Summary of performance limits	29
<b>4.2 Potential for improvements</b>	<b>29</b>
<b>1.3 Open issues and required R&amp;D</b>	<b>31</b>
<b>1.4 Comments on lifetime, maintainability, reliability</b>	<b>31</b>
<b>CHAPTER 5 – SUMMARY AND CONCLUSIONS</b>	<b>33</b>
<b>5.1 Summary</b>	<b>33</b>

**5.2 Conclusions**

**35**

**REFERENCES**

**37**

## List of Tables

Table 1: Approximate main dimensions of divertor cassette .....	3
Table 2: PPA divertor components cooling channel layout.....	4
Table 3: Power to divertor basic assumptions.....	6
Table 4: Definition of normalised power profiles at target plates .....	6
Table 5: Physical properties of tungsten alloy .....	7
Table 6: Physical properties of molybdenum alloy (TZM).....	7
Table 7: Allowable stresses in MPa (3Sm-values) for W1%La <sub>2</sub> O <sub>3</sub> and TZM.....	8
Table 8: Achievable heat transfer coefficients for helium cooling, summary.....	12
Table 9: Reference overall divertor cooling parameters .....	18
Table 10: Key thermal-hydraulic data for divertor components (Reference case) .....	19
Table 11: Parametric study of divertor coolant variables .....	20
Table 12: Cases investigated in thermomechanical analysis .....	24
Table 13: Temperatures at distinct points in cross section at y=0.4 m .....	25
Table 14: V. Mises equivalent stresses at distinct points in cross section at y=0.4 m.....	25
Table 15: Thermal deformation of divertor cooling channels.....	26
Table 16: Heat flux limits in MW/m <sup>2</sup> for target plates made from TZM and W alloy .....	29

## List of Figures

Figure 1: PPA divertor arrangement, single-null, at bottom of vacuum chamber.....	39
Figure 2: Schematic of PPA divertor cassette indicating main components and projected coolant routing.....	39
Figure 3: Possible PPA divertor flow diagram consisting of separate branches for inboard and outboard region .....	40
Figure 4: Normalised heat flux profile at vertical target plates (working hypothesis) .....	40
Figure 5: Heat transfer coefficient in smooth tubes for different inner diameters, D, and helium pressures, p .....	41
Figure 6: Evolution of porous media heat exchanger design .....	41
Figure 7: Typical cross section of a porous media target plate channel.....	42
Figure 8: Longitudinal section through target plate channel (length scaled-down to 1/10) .	42
Figure 9: Heat transfer and blower power dependence from inlet temperature.....	43
Figure 10: Heat transfer and blower power dependence from outlet temperature .....	43
Figure 11: Heat transfer and blower power dependence from inlet pressure .....	44
Figure 12: Heat transfer and blower power dependence from channel diameters.....	44
Figure 13: Dependence of pressure drop and HTC from PM geometry.....	45
Figure 14: Dependence of pressure drop and HTC from surface heat flux.....	46
Figure 15: Axial profiles of helium temperature rise and superficial mass velocity .....	47
Figure 16: Axial profiles of helium temperature rise for reduced PM insert lengths .....	48
Figure 17: Temperature distribution in a TZM/W helium-cooled divertor channel.....	49
Figure 18: V. Mises stress distribution in a TZM/W helium-cooled divertor channel .....	50
Figure 19: V. Mises stress distribution in a TZM/W helium-cooled divertor channel .....	51
Figure 20: Comparison of v. Mises stress distribution in W/W (left) and TZM/W (right) divertor channel.....	52
Figure 21: Thermal deflection of TZM/W divertor channel with 2- and 3-point support.....	52
Figure 22: Temperature at distinct points of TZM/W divertor channel vs. peak heat flux.....	53
Figure 23: Temperature at distinct points of W/W divertor channel vs. peak heat flux.....	53
Figure 24: V. Mises stress at distinct points of TZM/W divertor channel vs. peak heat flux ..	54
Figure 25: V. Mises stress at distinct points of W/W divertor channel vs. peak heat flux .....	54
Figure 26: Thermal deflection of TZM/W divertor channel vs. peak heat flux .....	55
Figure 27: Sensitivity of heat flux limit on various parameters.....	56





## Chapter 1 - Introduction

High Heat Flux Components (HHFC) developed in the past focused on water cooling with typical heat loads of  $20 \text{ MW/m}^2$  and up to  $30 \text{ MW/m}^2$  [1] for steady state operation. They were based on copper alloys with their exceptionally high thermal conductivity as structural material. This implied that the maximum temperature in the coolant confining structure (often referred to as the heat sink) had to be kept below about  $450 \text{ }^\circ\text{C}$ . And this, in turn, meant that the coolant temperature was limited (typically for water about  $140\text{--}160 \text{ }^\circ\text{C}$ ), making the system unattractive for power conversion.

The present aim in the frame of the European Programme “Preparation of a Power Plant conceptual Study, Plant Availability, PPA” is to exploit helium cooling of HHFCs (Task PPA1.3) with the special features of producing high-grade heat (for the benefit of power conversion), compatibility with helium-cooled blanket systems (economics), and its inert nature (avoiding chemical reaction hazards). Especially the high-grade heat calls for elevated coolant temperature, requiring the use of refractory alloys as structural materials. Thus, the objective of this task is to explore the manageable heat flux limits of helium-cooled divertor concepts that combine high thermal conductivity and high temperature resistant materials, good wall-to-coolant heat transfer characteristics and adequate coolant parameters, i.e., temperature, pressure and friction losses.

A major problem with gas cooling is the poor wall-to-coolant heat transfer coefficient (HTC) on the order of  $5000\text{--}10,000 \text{ W/(m}^2\text{K)}$  that can be achieved with smooth channels at reasonable pressure drop, as design studies have shown [2], [3]. This is up to an order of magnitude less than HTCs obtained with water cooling under subcooled flow boiling conditions [4], [5], [6]. To give an example, a HTC of  $5000 \text{ W/(m}^2\text{K)}$  and a heat flux at the cooling channel wall of  $5 \text{ MW/m}^2$  would result in a wall-to-coolant temperature difference of  $1000 \text{ K}$ . Consequently, researchers have looked for heat transfer enhancement methods for gas cooling of what is considered as conventional type, like roughening, fins, twisted tapes, grooves, other turbulence promoters [7], and of unconventional type that promise even higher performance, like the porous media (PM) concept [8], [9], jet impingement [10], or combinations of any kind. Thus, the task of helium-cooled divertors within PPA has been divided into two subtasks, one reviewing conventional design concepts and the other one addressing unconventional types. This report deals with the unconventional helium-cooled divertor, especially with the porous media concept.

Nevertheless, striving for high heat transfer coefficient is only one (although important) aspect in divertor design. Integrating the elementary cooling scheme into an overall divertor concept as part of a power plant needs further considerations. Therefore, this report starts in Chapter 2 with an overview of the main design constraints or assumptions in terms of general divertor configuration, dimensions, operating conditions, material choice, and other features, which give the rationale for the concept investigated. This concept is regarded as a viable and representative solution for the given set of constraints and is as such the proposed concept in the frame of this study, where many details have still to be worked out. The type, volume and results of the analysis performed for the proposed divertor design are described in Chapter 3, which lead to the performance limits summarised in Chapter 4. Here, also the deficiencies and open issues will be addressed. Summary and conclusions are drawn in Chapter 5.



## Chapter 2 - Overall Divertor Design Considerations

Roughly speaking, the divertor receives about 10 of 15 % of the gross thermal power in a tokamak machine. This is enough to be attractive for use in the power conversion system in order to enhance the plant efficiency. The heat to be removed from the divertor is very unevenly distributed over the individual sub-components, what depends on the configuration and on the mode of plasma operation. Most of the heat occurs as surface heat flux with a pronounced peaked profile, especially at the target plates, but a substantial fraction is deposited as a wide-spread surface and/or volumetric heat in the rest of the divertor components. At the present state of the PPA study neither the size of the machine, nor the power to the divertor – not to speak of the design and power distribution – are known. In order to yet give an idea of how the divertor might look like, we picture the ITER divertor configuration [11], scale it up to PPA reference dimensions [12], (which are considered also as a preliminary working hypothesis), assign power levels to individual components and fit a cooling system to the entire divertor. This gives us the boundary conditions to work out and assess details of the target plates, which are considered as the critical parts of the whole divertor arrangement. In the following subsections 2.1 through 2.3 these overall design guide lines and assumptions will be described, the candidate materials will be characterised, and the rationale for the target plate design will be outlined.

### 2.1 Assumptions on divertor configuration and operating conditions

#### 2.1.1 Main dimensions

Given the main dimensions and the shape of the plasma from systems analyses [12] and the necessary space required for the blanket, a first sketch can be drawn of the vacuum vessel surrounding everything, including the divertor (Figure 1). A single-null divertor, located at the bottom of the tokamak has been chosen for the PPA study. With the plasma major radius set at 8.1 m the separatrix may strike the outboard and inboard target plates at distances from the torus centre line of 8.9 m and 6.1 m, respectively.

A more detailed representation of the possible divertor cassette is shown in Figure 2, which is similar to the ITER design. The whole circular arrangement is supposed to be made up out of 48 cassettes, i.e., three per 1/16 torus sector. This results in the main dimensions given in Table 1. Figure 2 shows also the main components of the cassette which need active cooling, like vertical targets, dump target, dome, liners of the neutral gas chambers, etc. The casing serves as the integrating structure in which cooling channels, manifolds to the components, and exhaust channels are incorporated.

**Table 1: Approximate main dimensions of divertor cassette**

Number of cassettes for full divertor ring	48
Length of cassette (in radial direction)	5.5 m
Height of cassette	2 m
Width of cassette in toroidal direction min/max	0.7 m/1.4 m
Radius of strike points at outer/inner target plate	8.9 m/6.1 m
Length of outboard vertical target plate	1.6 m
Total weight of cassette (estimate)	150 kN

#### 2.1.2 Assumed cooling scheme

Defining the main dimensions allows a first projection of the coolant routing through individual components and, once the power distribution is known, thermal-hydraulics layout can be performed. Figure 3 depicts a possible coolant flow scheme in a divertor cassette. It consists of two branches, one for the outboard divertor region and one for the inboard. In each branch the coolant is routed first through the components with relatively low heat loads,

like the structure, dome, gas box liner, dump target, and finally through the heavily loaded target plate. The rationale for this scheme is explained in section 2.3 on page 9.

Each component comprises a number of parallel channels of certain length and size, which are connected to common inlet and outlet manifolds. Based on the scaled dimensions from Figure 2 and assumption on power distribution according to section 2.1.3, a set of parameters has been established in Table 2 below for first thermal-hydraulic estimates (for results see section 3.2). These parameters serve as orientation marks and are subject to optimisation.

**Table 2: PPA divertor components cooling channel layout**

	Component	Number of parallel channels	Number of channel layers	Channel length (m)	Channel diameter (m)	Power fraction <sup>a)</sup> to component
1.0	Outboard components					
1.1	Outboard main feed pipe	1	1	35	0.12	0
1.2	Outboard structure	12	3	4.0	0.03	0.02
1.3	Connection 1.2 to 1.4	12	2	2.2	0.03	0
1.4	Outboard central structure	12	2	3.0	0.03	0.02
1.5	Outer dome (half) and wing	44	1	0.8	0.018	0.16
1.6	Outer gas box liner	44	1	2.6	0.018	0.3
1.7	Outer dump target	32	1	0.4	0.028	0.08
1.8	Outer vertical target	32	1	2.2	0.028	0.42
1.9	Outboard main outlet	1	1	35	0.15	0
2.0	Inboard components					
2.1	Inboard main feed pipe	1	1	40	0.1	0
2.2	Inboard structure	8	2	3.0	0.03	0.02
2.3	Connection 2.2 to 2.4	8	2	2.2	0.03	0
2.4	Inboard central structure	8	2	3.0	0.03	0.02
2.5	Inner dome (half) and wing	42	1	0.8	0.018	0.16
2.6	Inner gas box liner	38	1	2.6	0.018	0.3
2.7	Inner dump target	22	1	0.4	0.028	0.08
2.8	Inner vertical target	22	1	1.9	0.028	0.42
2.9	Inboard main outlet	1	1	40	0.12	0

<sup>a)</sup> Fractions refer to outboard region and inboard region, respectively

## 2.1.3 Power to divertor and spatial distribution

### 2.1.3.1 Total power to divertor

The total power delivered to the divertor,  $P_{divertor}$ , can be estimated from fusion power,  $P_{fusion}$ , plasma heating power,  $P_{heating}$ , and neutron power generated in the divertor,  $P_{neutron,div}$ , according to equation (1-1).

$$P_{divertor} = (0.2 \cdot P_{fusion} + P_{heating}) \cdot F_{\alpha} + P_{neutron,div} \quad (1-1)$$

The fraction,  $F_{\alpha}$ , of the alpha plus heating power (first term in equation (1-1)) that goes to the divertor depends on plasma engineering and is usually accepted to range between 1/3 and 2/3. We assume the mean of this range,  $F_{\alpha} = 0.5$ . The other power values come from systems and neutronics analyses [12] (compare Table 3 on page 6) so that the total power to divertor during steady state operation results as  $P_{divertor} = 670$  MW.

### 2.1.3.2 Power sharing between outboard and inboard region

Equally uncertain as the fraction  $F_\alpha$  is the sharing of the total divertor power between the outboard and the inboard region. Again, this division can be influenced by plasma control. In the ITER final design report [11] a ratio of between 1/1 and 2/1 has been considered. Here we assume a sharing equal to the ratio of the outer-to-inner strike point radii, i.e.,  $8.9/6.1=1.46$ . With this, the total power to divertor is shared between the outboard and inboard region as 400 MW and 270 MW, respectively.

### 2.1.3.3 Power to divertor components

A third level of power division has to be established to individual divertor components. This needs detailed analyses of plasma physics, divertor physics and neutronics, which is beyond the scope of this study. As a first orientation we, therefore, adopt the division used in [11] for the detached plasma condition with minor modifications. The power fractions chosen are listed in the last column of Table 2 on page 4. Of special relevance to the target plate design is the distinction between the power fraction to target plates (42 %) and to the rest of the divertor (58 %) in each region at outboard and inboard. Thus, the linear power at the target plates per meter of toroidal length amounts to 3 MW/m.

### 2.1.3.4 Power profile at vertical target plates

Finally, assumptions need to be made about the power distribution at individual components. Here we restrict ourselves to discuss the power profile at the vertical target plates and presume that the local power levels in the rest of the divertor are uncritical. For the vertical target plates two poloidal power profiles have been defined in a PPA1.3 Task Meeting as working hypothesis:

- i) rectangular (flat) profile over 0.6 m poloidal length
- ii) peaked profile over 1.0 m poloidal length.

The normalised poloidal power profiles are specified in Table 4 on page 6, where normalisation is done as to obtain peak values of 1 in both cases. The flat profile (i) is the idealised case where the thermal power is dissipated uniformly through radiative mechanisms over a large portion of the target plates. The assumed length of 0.6 m is somewhat arbitrary. The peaked profile represents a more realistic distribution. It has been designed from the reference heat flux profile considered for ITER for an attached plasma regime by intuitively spreading it so that the peak value is reduced to one quarter while the integral power underneath the curve remains unchanged. This spread profile is assumed to better represent the detached plasma regime and is illustrated in Figure 4. The integral underneath the normalised profile results as 0.6 m for the flat profile and 0.326 m for the peaked profile. Hence, with a linear power at the target plates per meter of toroidal length of 3 MW/m from paragraph 2.1.3.3 we would obtain peak heat fluxes of  $3/0.6=5 \text{ MW/m}^2$  for the flat case and  $3/0.326=9.2 \text{ MW/m}^2$  for the peaked case.

### 2.1.3.5 Conclusion to power to divertor assumptions

Given the total fusion power of 3607 MW, the divertor has to be designed for a total power to divertor of 670 MW, leading (with the projected geometry and inboard/outboard division) to a linear power of 3 MW/m of toroidal length at the target plates. The corresponding peak heat fluxes would be  $5 \text{ MW/m}^2$  in case of a flat power profile and  $9.2 \text{ MW/m}^2$  for the peaked profile. These numbers scale almost linearly with fusion power if the geometry remains unchanged. Large uncertainties result further from unknown divertor performance with view to power sharing between inboard and outboard, power sharing between divertor components, and power profile at target plates. Thus, power values summarised in Table 3 below are considered as working hypothesis.

**Table 3: Power to divertor basic assumptions**

Total fusion power	3607 MW
Plasma heating power	122 MW
Neutron power to divertor	250 MW
Fraction of alpha + heating power to divertor	0.5
Total divertor power (rounded) from equation (1-1)	670 MW
Power sharing ratio between outer/inner divertor region	1.46/1
Linear power (toroidally) at target plates	3 MW/m
Peak heat flux at target plates (flat profile)	5 MW/m <sup>2</sup>
Peak heat flux at target plates (peaked profile)	9.2 MW/m <sup>2</sup>

**Table 4: Definition of normalised power profiles at target plates (working hypothesis)**

Distance from separatrix strike point, y (cm)	Rectangular profile ordinate (AU)	Peaked profile ordinate (AU)
-20.0	0	0
-16.0	0	0.007
-13.5	0	0.017
-10.0	1	0.04
-8.0	1	0.072
-5.5	1	0.152
-4.0	1	0.265
-1.5	1	0.58
0.0	1	0.86
1.3	1	0.992
2.0	1	1.0
4.0	1	0.992
8.0	1	0.925
14.0	1	0.779
21.0	1	0.598
27.0	1	0.476
33.7	1	0.357
40.0	1	0.265
50.0	1	0.16
55.0	0	0.114
60.0	0	0.0806
70.0	0	0.03
76.5	0	0.012
80.0	0	0

## 2.2 Materials involved

### 2.2.1 General materials considerations

Tungsten (W) and W alloys are leading candidates for plasma-facing components due to their low sputtering rates and high thermal conductivity. They also have high temperature strengths and low thermal expansion coefficients and, therefore, seem also to be attractive as heat sink material for high heat flux components. A major concern with W alloys is with fabrication and joining difficulties and radiation-induced embrittlement issues. The latter suggest to use them at operating temperatures above 600-700 °C when used as heat sink structure with coolant-confining functions. There is hope that the ductile behaviour of refractory alloys can be improved by modifications in the microstructure through, e.g., TiC precipitates [13], La<sub>2</sub>O<sub>3</sub> additions [14] or by alloying, for instance with rhenium. At present, the qualification of W alloys as structural material is insufficient and credit must be given to future developments in the fields mentioned. As armour material on the other hand, W or W alloys are considered as the only option for divertor target plates in fusion power reactors.

Given tungsten as armour material, an alternative heat sink material should also have the favourable properties of W and an even better ductility, and a minimum of thermal expansion

mismatch with W to avoid bonding problems. Good fabricability is also an essential. With these requirements in mind, only molybdenum (Mo) or Mo alloys like TZM seem to be an alternative to W. Tantalum alloys (e.g., Ta-10%W) have also been briefly discussed in the PPA1.3 Group Meeting, but they have lower thermal conductivity and seem to be inferior to Mo alloys in the high temperature regime. So in summary only the structure/armour combinations W/W and Mo/W (or their alloys) are considered in this study for the divertor vertical target plates.

For the other components of the divertor assembly with low to moderate heat loads, ferritic martensitic steel or equivalent is assumed, allowing a structural temperature of up to about 650 °C.

Thus, the following operating temperature windows are considered acceptable in this work, where especially the lower limit for W and Mo, or their alloys, take some credit of future advances in reducing the embrittlement problem.

- Tungsten or tungsten alloy as armour material                                    600 °C – 1800 °C
- Tungsten or tungsten alloy as structural material                                600 °C – 1400 °C
- Molybdenum or molybdenum alloy as structural material                        600 °C – 1200 °C
- Ferritic martensitic steel as structural material                                    250 °C – 650 °C

## 2.2.2 Material data

The material data base is derived mainly from product specifications prepared by Plansee AG, Austria, for W alloys [14], and Mo alloys (here TZM) [15], and from data collected by Zolti [16]. The physical properties used in this study are given in Table 5 and Table 6 below.

**Table 5: Physical properties of tungsten alloy**

Temperature (°C)	Thermal Conductivity [14] (W/(mK))	Young's Modulus [16] (10 <sup>3</sup> MPa)	Poisson's Ratio [16]	Coefficient of thermal expansion [14] (10 <sup>-6</sup> K <sup>-1</sup> )
20	122 <sup>a)</sup>	400	0.3	4.6 <sup>a)</sup>
500	106	382	0.3	5.0
1000	99	362	0.3	5.3
1500	94	331	0.3	5.5
2000	90 <sup>a)</sup>	290	0.3	5.7 <sup>a)</sup>

<sup>a)</sup> Value is extrapolated

**Table 6: Physical properties of molybdenum alloy (TZM)**

Temperature (°C)	Thermal Conductivity [15] (W/(mK))	Young's Modulus [15] (10 <sup>3</sup> MPa)	Poisson's Ratio [16]	Coefficient of thermal expansion [16] (10 <sup>-6</sup> K <sup>-1</sup> )
20	125	300	0.33	5.3
500	115	260	0.32	5.6
1000	100	220	0.32	6.0
1500	87	140	0.32	6.5

The mechanical properties of refractory materials vary significantly with their microstructure, i.e., with the degree of deformation or recrystallisation.

For W alloy the yield strength (Rp0.2) and tensile strength (Rm) versus temperature curves according to [14] were applied (as agreed upon in the PPA1.3 Group Meeting) to evaluate the allowable stress limits (3Sm). The curves were obtained for swaged rods, 40 mm in diameter and are labelled as stress relieved.<sup>1</sup>

For the TZM, 60 % of the tensile strength of 1 mm thick sheets, 'stress-relief annealed', according to [15] were chosen in stress evaluation. The reduction factor of 0.6 is thought to account for size effects as indicated in the reference, and in part for recrystallisation weakening. The yield strength is not documented in [15] and has, therefore, been taken from [16]. The source data and the derived 3Sm-values are listed in Table 7.

**Table 7: Allowable stresses in MPa (3Sm-values) for W1%La<sub>2</sub>O<sub>3</sub> and TZM**

Temp. (°C)	W1%La <sub>2</sub> O <sub>3</sub>			TZM			
	Rm [14]	Rp0.2 [14]	3Sm <sup>a)</sup>	Rm [15]	0.6 Rm <sup>b)</sup>	Rp0.2 [16]	3Sm <sup>a)</sup>
20						600	
100							
200	755	530	755	1170	700	450	700
300			658	1000	600		600
400			562	970	582	425	582
500	465	430	465	920	552		552
600			443	900	540	350	540
700			421	870	522		522
800			398	810	486	300	486
900			376	750	450		450
1000	354	337	354	700	420	250	420
1100			332	600	360		360
1200	310	300	310	450	270		270
1300	275	265	275	300	c)		c)
1400	200	160	200	150			
1500	136	93	136	110			
1600			113	80			
1700			91	50			
1800	90	34	68	40			

a) 3Sm=Min(Rm, 2Rp0.2), linear interpolation for intermediate points.

b) Assumed reduction of Rm due to size effects.

c) Recrystallisation starts for TZM at 1200 °C.

<sup>1</sup> In [16] a range of tensile strength is given for recrystallised (lower boundary) and stress relieved (upper boundary) state, and the chosen curve runs close to the lower boundary.



## 2.3 Rationale for the design proposal

### 2.3.1 Review of heat transfer enhancement methods

#### 2.3.1.1 Scope of heat transfer review

There are numerous publications on heat transfer and heat transfer enhancement methods for all kinds of application, and recurring and comprehensive bibliography or reviews are published in the International Journal of Heat and Mass Transfer, for instance in [17] and [18]. Only a small fraction of these is relevant to high heat flux components application in fusion devices, in particular to gas-cooled systems. In the remaining studies, there is one group that addresses heat transfer enhancement methods of the conventional type based on promoting turbulence, like e.g., by means of ribbed ducts [19], baffled ducts [20], wavy passages [10] and [21], metal mesh [22], and swirl tubes [23]. These are subject to review in a different task of the PPA study (PPA1.3.1) and are not discussed here. The objective of this work is to look at unconventional heat transfer enhancement methods which have essentially in common that they enlarge the solid/fluid interface area by introducing porous media or patterns of micro-fins and/or micro-channels. Yet other exotic types are jet impingement and particle addition. Recent studies in this field of unconventional methods are briefly reviewed below, mainly with regard to achievable heat transfer coefficients. The review is preceded by examples of attainable heat transfer coefficients in smooth tubes for comparison.

#### 2.3.1.2 Heat transfer in smooth tubes

A computer program has been written to calculate heat transfer and pressure losses in smooth and ribbed tubes [2]. It is based on equations documented in the VDI-Wärmeatlas [24] and the equation for the heat transfer coefficient reads

$$h = \frac{k}{D} \cdot \frac{\frac{\xi}{8} \cdot (\text{Re} - 1000) \cdot \text{Pr}}{1 + 12.7 \sqrt{\frac{\xi}{8}} \cdot (\text{Pr}^{0.67} - 1)} \cdot \left[ 1 + \left( \frac{D}{l} \right)^{0.67} \right] \cdot K^* \quad (2-1)$$

where

$$\xi = (1.82 \cdot \log_{10}(\text{Re}) - 1.64)^{-2}$$

$$K^* = (T_{\text{fluid}} / T_{\text{wall}})^{0.45}$$

valid for:  $2300 \leq \text{Re} \leq 10^6$ ,  $0.5 \leq \text{Pr} \leq 10^4$ ,  $0 \leq D/l \leq 1$  and with

$h$	[W/(m <sup>2</sup> K)]	Heat transfer coefficient
$k$	[W/(mK)]	Thermal conductivity of the fluid
$D$	[m]	Tube inner diameter
Re	[1]	Reynolds number
Pr	[1]	Prandtl's number
$l$	[m]	Length of channel
$K^*$	[1]	Factor to correct for wall temperature
$T$	[K]	Temperature

A graphical representation of equation (2-1) as function of helium flow velocity is shown in Figure 5 for three sizes of tube inner diameter ( $D=1, 1.5,$  and  $2$  cm) and for two helium pressures ( $p=8$  and  $12$  MPa). It is seen that flow velocity and pressure are dominating parameters affecting the heat transfer coefficient. Also the channel diameter has some

impact, especially when extrapolating to small sizes. So, at high velocities of 100-200 m/s, heat transfer coefficients of 10,000-25,000 W/(m<sup>2</sup>K) seem to be achievable in smooth channels. The pressure drop in this regime is still manageable. This result may serve as a yard stick in assessing heat transfer performance of unconventional methods.

### 2.3.1.3 Heat transfer in unconventional designs

Several types of porous media heat exchangers have been evaluated for high heat flux cooling application by Lindemuth, Johnson and Rosenfeld [8]. The porous medium consisted of small spheres of about 0.46 mm diameter. Analytical models have been derived for heat transfer and coolant pressure drop as function of physical parameters and design geometry (compare section 3.1.2 on page 16). Several test articles have been fabricated and tested in order to experimentally confirm the analytical models. For a small flat test article of a few square centimeter of heated surface made out of copper, heat transfer coefficients of up to 267,000 W/(m<sup>2</sup>K) are reported for water flow. Measured overall heat transfer coefficients were typically only half the predicted values, but measured and predicted pressure drops were in good agreement. Application of the analytical tools to helium cooling is attempted in section 3.2.2.

Helium-cooled porous media heat exchangers have also been tested in the Sandia National Laboratories for use in ITER [9]. The first article tested in 1993 was of the porous core type (1 cm diameter, 7.6 cm long) with axial flow. An absorbed heat flux of 16 MW/m<sup>2</sup> was demonstrated and heat transfer coefficients of 5000 to 7000 W/(m<sup>2</sup>K) were inferred. Based on these results a second generation test article, featuring an array of short parallel cylindrical channels connected via manifolds, was built and tested. Heat transfer coefficients of 15,000 to 18,000 W/(m<sup>2</sup>K) were demonstrated in these tests, using 2 MPa helium gas. It was summarised that the potential for several times this capability appeared achievable by improved fabrication technology and development of lower pressure drop flow geometries.

Remark: These results pertain to low temperature (<450 °C) copper alloy design and will certainly be degraded when using refractory materials. Nevertheless, researchers are optimistic to reach 20,000 W/(m<sup>2</sup>K).

Chikh et.al. have done a numerical study of forced convection enhancement in an intermittently heated channel [25]. The use of porous blocks, mounted on the inside of the heated parts of the channel to improve the thermal performance has been investigated parametrically. It has been shown that the blocks may improve the heat transfer under certain circumstances. The work is interesting with view to the mathematical formulation of flows in porous bodies, but the porous block design does not seem to be superior in thermal performance for divertor application compared to the transverse ribbed ducts as, for instance, used in hypervaportrons and as were also investigated in [19].

Saddleback Aerospace in California offers in the internet high-performance water-cooled copper micro-impingement heat sinks with unparalleled low thermal resistance [26] (equivalent to an effective heat transfer coefficient of the order of 200,000 W/(m<sup>2</sup>K) with water). The same company is developing hexagonal array micro-channel cooling panels for high heat flux application in fusion devices. The panel is a sandwich type design consisting of (from rear to front side) inlet manifold, outlet manifold layer, micro-channel layer and grooved face sheet. It is intended to fabricate a test article with 2 cm x 5 cm cooled area out of tungsten, helium-cooled, to be tested in the Sandia e-beam test facility. Typical micro-channel dimensions in the hexagonal array are 0.1 mm wide by 1 mm deep. Thermal-mechanical analysis is in progress, but no information is available yet on thermal performance with helium cooling.

Lee and Vafai have performed a comparative analysis between jet impingement and micro-channel cooling [27]. The jet impingement cooling usually requires a very large coolant flow with relatively small pressure drop, while the micro-channel cooling is subject to large pressure drops. The performance of the two technologies has been compared at their individual optimal conditions. The analysis revealed that the performance of the jet

impingement can only compete with the micro-channels with proper treatment of the spent flow and for larger ( $>0.07 \text{ m} \times 0.07 \text{ m}$ ) target plate dimensions. A maximum heat removal capability of 2 to 5 MW/m<sup>2</sup> is reported for water cooling depending on target plate dimensions and other parameters. Equivalent heat transfer coefficients are not explicitly given but can be calculated by use of the thermal-hydraulics model presented. Several other works related to micro-channel cooling have been reviewed by the authors.

Baxi has evaluated helium cooling for fusion divertors, addressing especially manifold sizes and pumping power [7]. He included a variety of heat transfer enhancement techniques, among them, besides conventional types, unconventional types, i.e., jet impingement and an optimised fin arrangement (also termed as micro-fins with height of 5 mm, pitch of 1 mm, and thickness of 0.4 mm in a copper structure). For both types heat transfer coefficients of 40,000 W/(m<sup>2</sup>K) seem to be attainable at reasonable fluid flow conditions and pressure drop. However, manifolding will be very complex for large components. The surface heat flux in this study was envisaged to be 10 MW/m<sup>2</sup> for testing and 5 MW/m<sup>2</sup> for the ITER divertor design as of May 1993.

Lu evaluated the augmentation of heat transfer in a micro-cell aluminum honeycomb heat exchanger with air as forced convection cooling [28]. Applying his analytical results obtained for laminar (Re=2000) air flow and aluminum as structural material to a helium-cooled honeycomb made of tungsten, would yield typical heat transfer coefficients of 7000-13,000 W/(m<sup>2</sup>K), depending on the thickness of the honeycomb structure. (These values hold for Re=2000, hydraulic diameter of 1 mm, He flow velocity of 14 m/s.) The heat transfer coefficient can perhaps be improved in a turbulent flow regime to a limited extent until the pressure drop becomes excessive. So, for helium-cooled divertor application HTC's of the order 10,000-15,000 W/(m<sup>2</sup>K) seem to be achievable with a tungsten honeycomb heat exchanger. It should be noted that Lu's results of a comparison with open cell metal foam suggest that for forced air cooling metal honeycombs compete well against metal foams.

Hwang and Lui have measured the heat transfer in trapezoidal ducts with pin-fin array as used in internally cooled turbine blades [29]. The fluid was air at 20-60 °C, ~0.1 MPa. The authors report on peak Nusselt numbers of about 180 for Re=21,000, corresponding to HTC of approximately 120 W/(m<sup>2</sup>K). Extrapolation to Re~10<sup>5</sup>, much smaller hydraulic diameter (5 mm instead of 30 mm) and helium as fluid (with  $k=0.33 \text{ W/(mK)}$  instead of  $0.02 \text{ W/(mK)}$  for air) would lead to HTC~35,000 W/(m<sup>2</sup>K). This would be an attractive number for divertor application, however the extrapolation is highly speculative.

In a recent review of helium cooling for fusion application Baxi and Wong [30] prepared a table of several heat transfer enhancement methods, showing for each method the increase in HTC (factor  $h_x$ ) and in friction losses (factor  $f_x$ ) relative to a smooth surface. In addition to several conventional methods (swirl tubes, 2D roughening, 3D roughening, swirl rods, swirl rods with 2D roughening) and the types already covered in [7] (micro-fins and jet impingement) the authors refer to the porous media concept (with  $h_x=5$ ,  $f_x=20$ ) and to particulate addition ( $h_x=10$ ,  $f_x=30$ ). Both methods look attractive from heat transfer point of view but are very poor with respect to pressure loss. Hence, the proposal in that study concentrated on swirl rod with 2D roughness (with  $h_x=3.5$  and  $f_x=7$ ).

#### 2.3.1.4 Conclusions on heat transfer enhancement performance

Many heat transfer enhancement methods for helium cooling relative to smooth channel performance have been, and are being, investigated. Based on mainly first generation measurements and extrapolating predictions, quite attractive heat transfer coefficients of 15,000 up to 50,000 W/(m<sup>2</sup>K) appear to be achievable in principle (Table 8 below). Most of the methods, however, are not well suited for large surfaces as needed in divertor application, or require complicated manifolding systems. This is particularly true for micro-channels, honeycombs, and jet impingement. The particle addition does not seem to be practicable because of erosion and pumping problems. A further problem is raised by the fact that satisfactory results have been obtained so far only for low temperature systems with

high conductive materials like copper or aluminum. The performance of heat exchangers made from refractory materials needs to be proved with view to their different physical properties, fabricability, bonding techniques and durability. The best potential for divertor application among these unconventional systems is seen in the porous media concept or in the micro-channel/micro-fin concept with expected heat transfer coefficients of about 20,000 W/(m<sup>2</sup>K). But this is in the range where also conventional enhancement methods may be able to compete.

**Table 8: Achievable heat transfer coefficients for helium cooling, summary**

Heat transfer enhancement method	HTC (W/(m <sup>2</sup> K))	Reference and comments
Smooth tubes	10,000-25,000	Predicted, see section 2.3.1.2, serves for comparison only
Porous media, cross flow Porous media, circumferential flow	18,000 20,000-25,000	Rosenfeld [9], measured. Experts' expectation and extrapolated by Baxi [30] when $hx=5^a$ ) and assuming $HTC_{smooth}=5000$ W/(m <sup>2</sup> K)
Micro-channels	to be determined	Saddleback Aerospace [26], promise HTC of about 200,000 W/(m <sup>2</sup> K) for water cooling
Micro-fins	40,000	Baxi, predicted and measured [7]
Honeycomb	15,000	Lu [28], estimates based on analytical results
Pin-fin arrays	35,000	HTC widely extrapolated in this work from measurements by Hwang et.al. [29]
Jet impingement	40,000	Baxi predicted [7] based on Gordon and Cobonque [31]
Particulate addition	50,000	Baxi [30], when $hx=10^a$ ) and assuming $HTC_{smooth}=5000$ W/(m <sup>2</sup> K)

<sup>a)</sup>For explanation of  $hx$  see last paragraph of section 2.3.1.3

### 2.3.2 Selection of cooling method for target plates

From the very beginning of this task it was felt that work should concentrate on the porous medium (PM) heat exchanger concept because of the encouraging results obtained with water and helium cooling in first generation experiments as described in section 2.3.1.3 and in references [8] and [9]. In addition, this concept had gone through several design stages starting from simple porous core in a circular tube, via the tile design with an array of parallel PM-filled cylindrical channels, to the circumferential flow design (Figure 6). Also from the review of heat transfer enhancement methods it was concluded in section 2.3.1.4 that the greatest potential for divertor application among the unconventional systems is seen in the PM concept or in micro-channel/micro-fin designs. When comparing both methods, the PM seems to be the most flexible and straightforward concept in terms of fabricability and cost. For instance, the PM inserts (wicks) can be made from small packed spheres (as promoted by Thermacore Inc., Lancaster, Pennsylvania, USA) or from metallic foam (as pursued by Ultramet, Pacoima, California, USA).

As a consequence, the PM concept has been selected in this study as reference design adopting the circumferential flow scheme according to version (d) in Figure 6. This has the advantage over version (c) that the region of peak heat flux gets fresh coolant at target plate inlet temperature and the flow path length is halved. In any case a firm bonding between the PM layer and the structure has to be assured, otherwise a propagating damage may occur.

### 2.3.3 Target plate design and operational window

The divertor target plates are envisaged to be slightly bent structures, following the contour of the cross section of the PPA divertor cassette as shown in Figure 2. Thus they are typically 1.6 m x 1.16 m at the outboard and 1.3 m x 0.8 m at the inboard. These plates are assumed to consist of arrays of separate channels, with minimal gaps in between, running in poloidal direction and being supported at the ends and at intermediate supports if needed. Groups of channels (or all channels of a plate) are connected to manifolds at the ends to provide inlet and outlet ports for the helium coolant. Free thermal expansion must be allowed in longitudinal (poloidal) direction relative to the supporting backbone, but only small out-of-plane deflections can be tolerated, especially differential deflections between neighbouring channels. To this end the target plate design is limited to this conceptual scheme, and the considerations concentrate on a single channel structure of 1.6 m length needed at the outboard as described below.

A typical cross section of the channel structure based on first order parametric studies is depicted in Figure 7. The lengthwise variation of the cross section necessary to accommodate the tilted and bent shape of the target plate surface is rather small at the outboard (ca. 4 % toroidally) and has thus been ignored. So the cross section of the divertor channel structure measures typically 36 mm x 39 mm and has a 28 mm diameter bore over the entire channel length.

The internals consist of the PM wick and two staggered and slit coolant tubes for helium inlet and outlet. Hence, the helium flow is forced from the inner tube via the upper slot into the wick, passes the wick circumferentially in two halves and exits via the sickle-shaped gap between the two tubes. The whole insert extends across the heavily loaded channel part only, i.e., approximately 0.6 m. The inlet tube should be tapered in order to balance flow velocities in longitudinal direction as schematically illustrated in Figure 8.

The insert and channel structure are assumed to be made from the same material, namely molybdenum or tungsten alloy as described in section 2.2 to minimise differential thermal expansion. Firm bonding between the outer wick contour and the structure is essential for optimal thermal conduction, whereas the inner contact may be loose, perhaps even sliding at one end. The decreasing pressure, when going from the inlet tube across the wick to the outlet tube, tends to open up the tubes at the upper slit and to squeeze the outlet tube at the back side. Therefore the opening shown at the rear side of the outlet tube may be a discontinuous slit or an array of holes.

The armour layer made of tungsten is attached to the channel structure, presumably by hot isostatic pressing (HIP). It is castellated in axial direction (slots at every about 30 mm) in order to avoid extra thermal stresses. The armour thickness is arbitrarily set to 3 mm, the actually required thickness has to be determined later. If it is in the range of a few millimeters, chemical vapour deposition can also be considered as plating method.

The back of the channel structure has been drawn as a flat face, enabling any kind of fixation to the backbone like studs, keys, bolts etc. The thickness and shape in that region has little impact on the thermomechanical behaviour as long as gross deflections need to be suppressed anyway (see section 3.2.3 on page 24).



## Chapter 3 - Analysis of proposed concept

### 3.1 Type of analysis and methods used

In accordance with the main objective of this task to assess the performance limits of unconventional helium-cooled divertors for power reactors (but not to work out an engineering design), the analysis is limited to a few issues considered as generic. The concept used should, therefore, be regarded as typical example with the need for further optimisation once more definite performance requirements have been established. The analysis comprises three fields:

- The overall divertor cooling parameters being responsible for the integration of the divertor cooling system into the plant power conversion concept.
- Thermal-hydraulics analysis of the target plates as the critical divertor components that drive main cooling parameters and hence, boundary conditions for the thermomechanics.
- Thermomechanical analysis of the target plate in terms of stress and strains as the ultimate, but not necessarily the only, performance limit of high heat flux components.

The methods and basic assumptions applied in these three fields of analysis are described in the subsections below. The results will then be discussed in section 3.2.

#### 3.1.1 Outline of overall divertor cooling assessment

The conceptual design of the divertor adopted has already been described in Chapter 2 in terms of main dimensions, cooling scheme and spatial power distribution. In order to easily perform a parametric study on key thermal-hydraulic variables like mass flow rate, pressure drop, temperature rise in each of the divertor components and in the divertor cooling system as a whole, a special purpose personal computer program "DIVERTOR" has been set up in SPEAKEASY language [32].

DIVERTOR calculates at first the thermal power going to the outboard and inboard divertor region based on the total power to divertor (see section 2.1.3.1) and on the power sharing assumptions (sections 2.1.3.2 and 2.1.3.3 on page 5). The calculation is then made for a single divertor cassette (1/48 sector) in which the inboard and outboard regions are served separately and comprise nine components each (Table 2 on page 4), which are passed by the coolant in series. Each component in turn has a number of parallel coolant channels, sometimes in more than one layer, that are connected to sub-headers. The channel length of each component is estimated from the divertor geometry. The feed and return pipes run essentially external to the vacuum vessel and their lengths account for the main ring headers supplying all or a group of cassettes.

The diameter assigned to each flow channel is subject to optimisation. Likewise the thermal-hydraulic parameters like inlet pressure and temperature and the desired overall temperature rise can be varied. Governing equations used in the fluid dynamics part of DIVERTOR are standard for incompressible flow in circular ducts with specified wall roughness, applying temperature dependent fluid (here helium) properties. Not included in this assessment are the main loop external to the main ring headers and the flow channel inserts as needed in the target plates (and perhaps in some other components). The latter are treated separately in section 3.2.2.

The output of DIVERTOR gives essentially the flow parameters at inlet and outlet of each divertor component, average fluid properties at each component, and pumping power as will be discussed in section 3.2.1 on page 18.

### 3.1.2 Outline of target plate thermal-hydraulics

As was shown in section 2.3.3, the target plate is assumed to consist of an array of parallel channels, 1.6 m long. Only a single channel with a porous medium insert is regarded here. For the flow in the porous medium the heat transfer and pressure drop correlations developed by Rosenfeld [8] were adopted which read for the overall convective heat transfer coefficient in the wick

$$h_0 = \varepsilon \cdot h_p + \sqrt{h_p \cdot k_p \cdot S_p} \quad (3-1)$$

In this model the local particle-to-fluid heat transfer coefficient,  $h_p$ , is expressed in the form

$$h_p = 1.064 \cdot \bar{c}_p \cdot G \cdot \left( \frac{\bar{c}_p \cdot \mu_f}{k_f} \right)^{-2/3} \cdot \text{Re}^{-0.41} \quad (3-2a)$$

for  $\text{Re} \geq 350$ , i.e., turbulent flow and

$$h_p = 18.1 \cdot \bar{c}_p \cdot G \cdot \left( \frac{\bar{c}_p \cdot \mu_f}{k_f} \right)^{-2/3} \cdot \text{Re}^{-1} \quad (3-2b)$$

for  $\text{Re} \leq 40$ , i.e., laminar flow,

where the Reynolds number is defined by use of the superficial mass velocity and the particle diameter:

$$\text{Re} = \frac{G \cdot D_p}{\mu_f} \quad (3-3)$$

$\varepsilon$		Porosity of wick
$k_p$	W/(mK)	Thermal conductivity of wick
$S_p$	m <sup>2</sup> /m <sup>3</sup>	Specific surface of wick
$\bar{c}_p$	Ws/(kg K)	Specific heat of fluid at mean temperature
$G$	kg/(m <sup>2</sup> s)	Superficial mass velocity in wick
$\mu_f$	kg/(ms)	Dynamic viscosity of fluid
$k_f$	W/(mK)	Thermal conductivity of fluid
$D_p$	m	Particle diameter of wick

The pressure drop equation reads

$$\frac{\Delta p}{\Delta l} = \frac{G}{\rho_f \cdot D_p} \cdot \frac{(1-\varepsilon)}{\varepsilon^3} \cdot \left( \frac{150 \cdot (1-\varepsilon) \cdot \mu_f}{D_p} + 1.75 \cdot G \right) \quad (3-4)$$

where additionally

$\Delta l$	m	flow path length in wick
$\rho_f$	kg/m <sup>3</sup>	fluid density

The thermal-hydraulics analysis was performed in two steps, using special SPEAKEASY programs, i.e.,



- parametric study assuming a flat heat flux profile to investigate the influence of geometrical and flow parameters on pressure drop and heat transfer,
- refined analysis applying a peaked power profile to assess the flow redistribution in longitudinal direction due to varying fluid properties.

In the one-dimensional parametric study the model assumes a uniform heat load along the channel axis and is thus independent on channel length. It needs as input parameters the dimensions of the channel cross section ( $r$ ,  $R$ ,  $w_M$  as defined in Figure 7), the wick characteristics ( $\varepsilon$ ,  $k_p$ ,  $S_p$ ,  $D_p$ ), the linear power per unit toroidal length, and the coolant parameters. The coolant properties are taken at the mean coolant bulk temperature,  $\bar{T}$ , which is simply  $\bar{T} = T_{in} + 0.5 \cdot \Delta T$  with  $\Delta T$  = temperature rise in the wick. The model ignores the pressure drop occurring in the inlet and outlet tube.

The quasi two-dimensional refined analysis with peaked power profile considers the variation in flow resistance along the channel axis,  $y$ , and thereby a feedback on flow rate and coolant temperature rise distribution. As boundary condition the pressure at the inlet to the wick annulus was kept constant along  $y$ . At the outlet from the wick the pressure was also assumed to be constant along  $y$ , but its value was iterated as to achieve a pressure drop and integral mass flow rate needed to obtain a given mean temperature rise. Again the pressure drop occurring in the inlet and outlet tubes was ignored. For the axial heat load distribution the normalised profile specified in Figure 4 in the interval  $-0.2m \leq y \leq 0.8m$  was applied, i.e., the porous medium insert length was assumed to be 1 m.

### 3.1.3 Outline of thermomechanical analysis

The mechanical analysis of the divertor channel has been performed with the computer program PERMAS. It is a finite element code, compatible with the CATIA CAD-system. PERMAS is capable of using temperature dependent material property data. The data for tungsten and molybdenum alloys as specified in Table 5 and Table 6 are taken with linear interpolation within temperature intervals.

The 3D model of the channel structure includes the armour layer, but it ignores the porous medium insert and tubes. The calculation is done in two steps: (i) the temperature distribution is calculated for the power applied to the heated surface as specified in Figure 4, a constant coolant temperature (generally 630 °C), and a constant heat transfer coefficient throughout the channel inner wall (20,000 W/(m<sup>2</sup>K)). The other surfaces are adiabatic. (ii) Elastic stresses and strains are then computed as a result of the thermal load from step (i) and internal pressure. Two different support conditions are applied, namely a 2-point support at  $y=0$  and  $y=1.6$  m, and a 3-point support at  $y=0$ , 0.6, and 1.6 m. For this step the armour layer has been ignored because its castellation is supposed to minimise extra stiffness.

#### Remarks:

Support means free to expand in  $y$ -direction but restrained perpendicular to  $y$ -direction.

A special case with all axial nodes supported has been investigated additionally, which would suppress any deflection perpendicular to the  $y$ -direction.

The narrow castellation slots in the armour layer may cause local stress concentration, which has not been regarded here.

## 3.2 Analysis results

### 3.2.1 Overall divertor cooling parameters

#### 3.2.1.1 Rationale for divertor cooling parameters

The results of divertor cooling parameters discussed in this section are based on a set of fundamental assumptions, which represent just one of many possible ways of cooling the individual divertor components. The rationale of the assumptions is as follows:

- The inboard and outboard region of each cassette is served by separate supply lines in order to enable for adjustment of varying inboard/outboard power sharing.
- Divertor components within each region are served in series (except for parallel channels pertaining to the same component) to keep the number of main supply lines small and to simplify external circuitry (compare the flow diagram in Figure 3).
- Flow channel size in each component has been chosen with view to the component's function, i.e., whether it receives mainly surface heat flux (many small channels) or volumetric heat (few medium size channels) or no heat (single large channel) as listed in Table 2 on page 4.
- Optimisation of main cooling parameters aimed at meeting the materials temperature windows (section 2.2.1 on page 6), getting attractive conditions for power conversion, keeping the pumping power low, and obtaining high heat transfer coefficients in channels.
- All flow channels are assumed as plain ducts (roughness 50 micrometers) without any heat transfer enhancement inserts, which definitely are needed in the target plates as analysed in section 3.2.2 and perhaps in a simpler form in some other components like in the dome.

#### 3.2.1.2 Reference divertor cooling parameters

As result of the parametric study described in section 3.2.1.3, and keeping in mind the layout rationale outlined in the last section, the reference parameters for the divertor cooling system according to Table 9 have been selected for further analyses.

**Table 9: Reference overall divertor cooling parameters**

Helium inlet temperature	400 °C
Helium outlet temperature	800 °C
Helium inlet temperature to target plates	632 °C
Helium pressure at divertor inlet	8 MPa
Pressure drop in outboard divertor region <sup>a)</sup>	0.18 MPa
Pressure drop in inboard divertor region <sup>a)</sup>	0.2 MPa
Total mass flow rate	323 kg/s
Ratio of blower power to divertor thermal power <sup>a)</sup>	0.016

<sup>a)</sup> This does not include losses from inserts, see section 3.2.2

The coolant temperatures are attractive for power conversion. When using an independent secondary closed loop gas cycle (Brayton cycle with turbine, recuperator and three-stage compression), an overall conversion efficiency, including the primary circulator power, of approximately 48 % can be reached, equivalent to 325 MW<sub>el</sub> power from the divertor cooling system. If, on the other hand, the divertor heat is merged into the blanket cooling system at lower temperature levels, the gain in electrical output would be less, e.g., about 200 MW<sub>el</sub> at conditions of the improved helium-cooled pebble bed blanket according to [33].

The inlet temperature to the target plates is 632 °C. This is at the same time the minimum temperature of the target plate structure in thermal equilibrium in regions of low thermal load, i.e., at the inlet to the channels and at their backs. Most parts of the target plates, in particular where the loads are high, operate at much higher temperatures as will be shown in section 3.2.3.

The system pressure of 8 MPa is moderate. It is a compromise between pumping power on one hand, and minimising primary stress in target plate channels and in other components. Hence, the pressure drop of about 0.2 MPa is reasonably small leading to a ratio of blower power to divertor power of 1.6 % only. But losses from inserts need to be added.

Further distribution of key thermal-hydraulic parameters among individual divertor components is listed in Table 10 for the reference case. One can see that the flow velocities range from 28 to 76 m/s, Reynolds numbers from  $0.13 \times 10^6$  to  $1.24 \times 10^6$ , and heat transfer coefficients calculated by use of equation (2-1) are typically 3000 W/(m<sup>2</sup>K). In the dome and gas box liner it goes up to 4600 W/(m<sup>2</sup>K), which is intended (without having performed detailed analysis for these components).

**Table 10: Key thermal-hydraulic data for divertor components (Reference case)**

	Component	Temp. at inlet (°C)	Pressure drop (MPa)	Flow Velocity (m/s)	Reynolds Number ( $10^6$ )	Friction Factor	HTC (W/(m <sup>2</sup> K))
1.0	Outboard components	400	0.178				
1.1	Outboard main feed pipe	400	0.051	62	1.24	0.016	3000
1.2	Outboard structure	400	0.006	28	0.14	0.022	2100
1.3	Connection 1.2 to 1.4	408	0.008	42	0.21	0.022	2900
1.4	Outboard central structure	408	0.011	42	0.20	0.022	2900
1.5	Outer dome (half) and wing	416	0.014	68	0.18	0.026	4600
1.6	Outer gas box liner	480	0.051	76	0.17	0.026	4500
1.7	Outer dump target	600	0.002	48	0.14	0.023	3000
1.8	Outer vertical target	632	0.010	53	0.13	0.023	2700
1.9	Outboard main outlet	800	0.026	64	0.73	0.015	2100
2.0	Inboard components	400	0.197				
2.1	Inboard main feed pipe	400	0.071	61	1.02	0.017	3000
2.2	Inboard structure	400	0.012	43	0.21	0.022	2900
2.3	Connection 2.2 to 2.4	408	0.009	43	0.21	0.022	3000
2.4	Inboard central structure	408	0.012	44	0.21	0.022	2900
2.5	Inner dome (half) and wing	416	0.007	49	0.13	0.026	3500
2.6	Inner gas box liner	480	0.032	61	0.13	0.026	3700
2.7	Inner dump target	600	0.002	48	0.14	0.023	3000
2.8	Inner vertical target	632	0.008	53	0.13	0.023	2700
2.9	Inboard main outlet	800	0.045	69	0.62	0.016	2300

### 3.2.1.3 Parameter variation

To give a few examples of how the cooling system would react on changing some parameters relative to the reference case discussed in the previous section, Table 11 shows selected cases with one or two input parameters changed (shaded cells), sometimes to extreme and unrealistic values, like in cases 10 to 12.

A more systematic picture is given in Figure 9 to Figure 12. In all these figures only one input parameter was varied at a time (the one indicated at the abscissa). The term HTC means heat transfer coefficient in the outer dome taken as example (component 1.5 in Table 10), and blower/divertor power ratio means thermal blower power needed to overcome pressure losses in the cooling system up to and including the main ring headers but excluding losses in the target plate inserts, divided by the total divertor power listed in Table 3. The results of the parametric study are summarised as follows.

**Table 11: Parametric study of divertor coolant variables**

Case	Inlet Temp. (°C)	Outlet Temp. (°C)	Inlet Pressure (MPa)	Pressure Drop <sup>a)</sup> (MPa)	Mass Flow Rate (kg/s)	Blower/Divertor Power Ratio (%)
Reference	400	800	8	0.18	323	1.6
2	400	800	6	0.24	323	2.8
3	400	800	10	0.14	323	1.0
4	400	800	12	0.12	323	0.7
5	400	800	14	0.10	323	0.5
6	300	800	8	0.10	258	0.6
7	400	900	8	0.12	258	0.8
8	400	700	8	0.31	431	3.7
9	400	700	12	0.20	431	1.6
10	400	600	12	0.45	646	5.3
11	400	1200	14	0.03	161	0.07
12	400	1200	8	0.05	161	0.2

<sup>a)</sup> Refers to outboard region. In the inboard region it is about 10 % higher.

The blower power scales slightly more than linear with the inlet temperature, while the heat transfer coefficient (HTC) improves only very weakly with increasing inlet temperature (Figure 9). So, a low inlet temperature is preferable. The choice of 400 °C as reference value was dictated by the constraints of the target plate temperature.

There is a strong dependence of blower power from outlet temperature (i.e., overall temperature rise) as shown in Figure 10. When trying to keep the blower/divertor power ratio below about 2 % in order to have margin for losses generated by the inserts, one should choose the outlet temperature greater than 780 °C. On the other hand, it must not be driven too high with view to the target plate temperature window. Hence, the outlet temperature of 800 °C is a good choice with a fairly good HTC.

Similarly, the blower power shows a strong dependence on system pressure for values below about 6 MPa (Figure 11). Using the same argument as in the last paragraph, the reference pressure was set to 8 MPa. There is margin to further lower the blower power to about 1/3 of the reference value when going to an inlet pressure of 14 MPa, although at the expense of higher primary stresses. There is no impact of the pressure level on the heat transfer coefficient.

Finally, channel dimensions established in Table 2 on page 4 have a strong effect on blower power, and there are many ways to optimise channel diameters in individual components, once detailed requirements are known. The largest contribution come from the main feed and return pipes (positions 1.1, 1.9, 2.1 and 2.9 in Table 2 and Table 10) and from the gas box liner (positions 1.6 and 2.6). To simply illustrate the sensitivity of blower power and HTC on channel diameters a scaling factor of between 0.8 and 1.2 has been applied simultaneously to all components (Figure 12). This reflects the well known correlation between pressure drop and pipe diameter  $\Delta p \propto D^{4.8}$ . The HTC drops by 15 % when increasing the diameters by 10 %.

In summary to the overall divertor cooling parameter analysis one can conclude: Based on first assumptions for divertor configuration and coolant flow scheme, and considering temperature windows for target plates and other divertor components, the following reference values are chosen from the parameter study: Helium inlet/outlet temperature = 400 °C/800 °C, inlet pressure = 8 MPa (Table 9 on page 18). This results in low pumping power at reasonable heat transfer coefficients in channels that have no heat transfer enhancement. There is sufficient margin to optimise the pumping power, but there is

practically no margin to alter the helium temperatures under the restrictions assumed here. The key parameters are suited for an effective power conversion in a self-contained conversion system.

### 3.2.2 Thermal-hydraulics analysis of target plate

The porous media (PM) inserts in the target plate channels are major contributors to the total pressure loss in the system and need special attention. But above all, the main objective of the PM inserts is to enhance the heat transfer from the structure to the fluid. Given the PM insert of the circumferential flow type according to Figure 7, the design offers many options to optimise the geometry with respect to pressure drop and effective heat transfer coefficient (HTC). The most obvious parameters are the channel diameter,  $2R$ , the thickness of the wick,  $R-r$ , and the width of the channel structure,  $w_M$ . Also the character of the wick has a strong impact, represented by the variables: particle diameter,  $D_p$ , porosity,  $\varepsilon$ , thermal conductivity of the wick material,  $k_p$ , and specific surface,  $S_p$ , as defined in the model adopted (section 3.1.2 on page 16). To get an overview of the importance of these variables a 1D parametric study for a slice of a channel cross section was carried out as a first step, corresponding to a flat heat flux profile. The results of varying  $R$ ,  $R-r$ , and  $w_M$  are presented next. The quasi 2D analysis for a peaked power profile, but for a distinct geometry only, will then be addressed in section 3.2.2.2.

#### 3.2.2.1 One-dimensional parametric study on PM insert geometry

The influence of the porous media wick geometrical parameters on pressure drop,  $\Delta p_w$ , according to equation (3-4), and on the effective heat transfer coefficient,  $h_o$ , according to equation (3-1) is presented in Figure 13. The pressure drop is indicated at the left hand axis. It occurs in the wick at a helium mass flow rate that produces a helium temperature rise of 168 K (the projected reference temperature rise in the target plates from section 3.2.1.2) at a surface heat flux of  $5 \text{ MW/m}^2$  and constitutes therefore a reference condition, compatible with the overall divertor cooling system layout. The heat transfer coefficient shown at the right hand side in Figure 13 has been plotted as normalised function and shall only indicate the trend. This was done because the computed HTC using equations (3-1) to (3-3) has not been proved for helium flow and refractory materials, and appears to be much too high as was already discussed in section 2.3.1.3. For instance, the calculated HTC at reference conditions ( $G=34.4 \text{ kg/(m}^2\text{s)}$ ,  $R=0.014 \text{ m}$ ,  $R-r=0.003 \text{ m}$ ,  $w_M=0.036 \text{ m}$ ,  $k_p=10 \text{ W/(mK)}$ ) was found to be  $h_{0,Ref}=51,600 \text{ W/(m}^2\text{K)}$ , whereas the expected value is of the order  $20,000 \text{ W/(m}^2\text{K)}$  only. Nevertheless, the computed value,  $h_{0,Ref}$ , has been used to normalise all HTC curves in lieu of a better computational model. The following results were obtained.

Changing for example the *outer radius of the wick* between  $0.013 \text{ m}$  and  $0.015 \text{ m}$ , while keeping the wick thickness ( $R-r$ )= $0.003 \text{ m}$  constant, would increase the pressure drop from  $0.41 \text{ MPa}$  to  $0.48 \text{ MPa}$ . That means the pressure drop scales almost linear with  $R$ , which is simply the effect of enlarged flow path. On the other hand, the normalised HTC remains unchanged (Figure 13, top frame). It is to be noted that  $R$  should be chosen as large as possible within the limits set by the channel structure width,  $w_M$ , in order to enlarge the heat transfer surface between the structure and the wick. In this design,  $R=0.014 \text{ m}$  was selected as reference value leading to the nominal pressure drop of  $0.45 \text{ MPa}$ .

In Figure 13 centre we have changed the *inner radius of the wick* between  $r=0.01 \text{ m}$  and  $0.012 \text{ m}$ , while keeping the outer radius fixed at  $R=0.014 \text{ m}$ , i.e., the wick thickness ( $R-r$ ) was varied between  $0.004 \text{ m}$  and  $0.002 \text{ m}$ , respectively. This has a dramatic impact on the pressure drop, particularly for  $r>0.011 \text{ m}$  or  $(R-r)<0.003 \text{ m}$ . In contrast, the HTC is moderately affected. Hence, the choice of  $r=0.011 \text{ m}$  as reference value in the present design seems to be a good compromise between pressure drop and HTC.

Finally, the influence of the *channel structure width*,  $w_M$ , has been studied in a way as to scale  $R$  with  $w_M$  and keeping the wick thickness ( $R-r$ )= $0.003 \text{ m}$  constant (Figure 13, bottom). In this case the pressure drop almost doubles as  $w_M$  is increased by 25 %. This results from

two effects: first, the flow path length becomes larger and second, the total heat delivered to the channel is increased at constant surface heat flux, requiring a larger mass flow rate in order to maintain the same temperature rise of 168 K. The HTC profits a little from this latter effect. Again, it's mainly the pressure drop that led to the decision to take  $w_M=0.036$  m as reference design value.

So far we have investigated cases in which the surface heat flux and the temperature rise in the wick were kept constant at  $5 \text{ MW/m}^2$  and 168 K, respectively. We are now asking, how things would change if the surface heat flux was increased. In Figure 14 the surface heat flux was varied between 3 and  $10 \text{ MW/m}^2$ , and as parameter the wick inner radius,  $r$ , was introduced with  $r=0.011$ , 0.010, and 0.009 m, pertaining to curves from top to bottom. As the solid curves indicate, the pressure drop increases approximately as the square of the heat flux, which equation (3-4) does not show beforehand. However, the losses can be effectively brought back by enlarging the wick thickness, i.e., by reducing  $r$ . So, for instance, the reference value of 0.45 MPa (at  $r=0.011$  m and  $5 \text{ MW/m}^2$ ) can also be maintained at  $r=0.009$  m and  $8.6 \text{ MW/m}^2$ . The dependence of the normalised HTC from the surface heat flux is less sensitive as the group of dashed lines show (again for  $r=0.011$ , 0.010 and 0.009 m from top to bottom).

This analysis demonstrates that the wick dimensions can be optimal with regard to pressure drop and heat transfer only for a certain design point defined by the surface heat flux, coolant temperature rise and coolant pressure. Large deviations from the design point make the layout ineffective. This will be the case for strongly peaked power profiles at divertor target plates which brings us to the next problem of investigating the impact of non-uniform heat flux distribution along the channel axis.

### 3.2.2.2 The impact of non-uniform heat flux on thermal-hydraulics

The first step of analysing the PM divertor concept with circumferential flow was performed assuming a uniform heat load along the channel axis. If the heat load is non-uniform, the temperature distribution at the outlet from the PM annulus will assume an axial profile similar to the heat load distribution. Given a certain mean temperature rise for the whole channel of, say the reference value of 168 K, the local coolant temperature and thus, the temperature in the structure, may become very high. It was therefore investigated how close the coolant temperature rise profile would follow the heat load profile in its peak-to-average ratio. As boundary condition, the pressure at the inlet to the PM annulus was assumed to be uniform along the channel axis. At the outlet from the PM annulus the pressure was also kept constant along the axis, but its value was iterated as to achieve an integral mass flow rate needed to obtain the given mean temperature rise. The pressure drop in axial direction occurring in the feed and exit channel of the PM insert was ignored in this approach. For the axial heat load distribution the reference profile specified in Table 4 and Figure 4 was chosen with the peak heat flux of  $9.2 \text{ MW/m}^2$  (equivalent to a mean heat flux of  $3 \text{ MW/m}^2$  across the 1 m wide profile).

Starting from the reference case with:

- Mean temperature rise in the wick,  $DT=168$  K
- Peak heat flux,  $q_{\max}=9.2 \text{ MW/m}^2$
- Thickness of wick,  $(R-r)=0.003$  m
- Helium inlet temperature to the wick,  $T_{W,\text{in}}=632$  °C
- Pressure inlet to wick,  $p_{W,\text{in}}=8$  MPa

the analysis involved the variation of all of these parameters in reasonable ranges. A few selected trends are discussed below.

The calculated HTC decreases by about 20 % as the temperature rise in the wick increases from 100 to 200 K, due to the reduced mass flow rate and velocity. The deviation of the HTC in axial direction from its mean value is less than 1 %. With regard to absolute values of the HTC please refer to the discussion in section 3.2.2.1.

There is a strong influence of the mean temperature rise on the pressure drop in the wick. For  $DT < 100$  °C the pressure drop becomes prohibitive. On the other hand, at the reference temperature rise of  $DT = 168$  K and at  $q_{\max} = 9.2$  MW/m<sup>2</sup> the pressure drop is 0.18 MPa only. This is of course considerably lower than the value obtained for uniform heating at the same temperature rise, since in this case the PM insert is assumed to extend over the full profile width of 1 m in contrast to  $DY = 0.6$  m in the uniform heat load cases (see also description to Figure 16).

Figure 15 (top frame) shows the profile of the temperature rise in longitudinal direction given that the porous media insert extends over the whole length of the power profile between  $y = -0.2$  m and  $y = 0.8$  m. The mean temperature rise varies between 100 and 200 K. The peaking is very pronounced with peak-to-average values of 3.14, 3.21, 3.24, 3.29 for the cases with  $DT = 100, 150, 168$  and 200 K, respectively. This is little larger than the power peak-to-average value of 3.07.

The superficial mass velocity,  $G(y)$ , varies along the channel length due to changing temperature and fluid property data, especially density (Figure 15, bottom). This leads to a relative mass flow reduction at locations of high heat flux. For the reference case with an overall temperature rise of 168 K the reduction in superficial mass velocity at the point of peak heat flux (at  $y \sim 0.03$  m) is about 25 % compared to the low heat flux regions. The shape of the curves remains unchanged for different temperature rises.

In Figure 16 it is shown how the profile of the helium temperature rise will be affected if the length of the porous medium insert,  $DY$ , is changed, while the other parameters are kept at their reference values as listed above. The rationale behind this is that the PM insert is only needed in regions of high heat loads. For instance, chopping the heat flux profile in Figure 4 at normalised fluxes of less than 0.12 would require the PM insert to cover the section between  $y = -0.06$  m and  $y = 0.54$  m, i.e.,  $DY = 0.6$  m. Thus, one finds from Figure 16 that for full coverage of the power profile by the PM insert ( $DY = 1$  m) the maximum helium temperature rise amounts to  $\max \Delta T = 580$  K (which is a peak helium temperature of  $580 + 632 = 1212$  °C), whereas for  $DY = 0.6$  m  $\max \Delta T = 322$  K is obtained. It should be noted that for all curves the mean temperature rise in the whole channel was maintained at 168 K, however the mean  $\Delta T$  at the PM insert was reduced by the fraction of the integral power underneath the chopped power profile to the integral underneath the full power profile. The balance to  $\Delta T = 168$  K occurs in the chopped tails of the power curves.

Other observations are the following. With smaller wick thickness (reduced from 3 mm to 2 mm) the HTC goes up by 15 %. If the inlet temperature is changed between 700 and 300 °C the HTC is hardly affected. It decreases by 8 %. An even smaller influence has the system pressure. This is because the superficial mass velocity,  $G(y)$ , and the Reynolds number,  $Re(y)$ , which are the only flow parameters in the heat transfer equations (3-1) to (3-3), are unchanged at constant mean temperature rise.

Summarising the thermal-hydraulic analysis results for non-uniform heat load profiles one can state that for full coverage of the heat flux profile by the PM insert (here 1 m) the helium temperature rise experiences a similar profile as the incident heat load, leading to much higher local peak coolant temperatures (in the reference case 1212 °C) compared to the mean outlet temperature (800 °C). This is because the coolant is bypassed in axial regions of low power. Reducing the PM insert length to about 0.6 m helps a lot, but the problem of unknown fluctuations of the separatrix strike point becomes more prudent. Of course, the peak coolant temperature occurs theoretically only at the back of the annulus where the loads are small, but most of the heat is added already in the front region, which requires a more sophisticated and coupled model to combine thermal-hydraulics in the wick and heat conduction in the channel structure. By the way, the heat transport by the fluid in circumferential direction can help to reduce thermal stresses in the structure discussed next.

### 3.2.3 Thermomechanical analysis of target plate

After several scope studies the thermomechanical analysis with the finite element code PERMAS (compare section 3.1.3 on page 17) focused on a few cases in which the material combination of the divertor channel (tungsten as structure combined with tungsten as armour layer versus molybdenum alloy as structure protected by a tungsten armour layer), the heat load (5 and 10 MW/m<sup>2</sup> peak load using the load profile shown in Figure 4) and the type of channel fixation (denoted as 2-point and 3-point support, and the special case 2a with all nodes being supported) were investigated. The following Table 12 gives an overview of the combinations studied. Main results are discussed below.

**Table 12: Cases investigated in thermomechanical analysis**

Case	Material Combination		Peak Heat Flux (MW/m <sup>2</sup> )	Number of Support Points	See Figure(s)
	Structure	Armour			
1	TZM	W	5	2	17, 18, 20
2	TZM	W	5	3	17, 19, 20, 21
2a	TZM	W	5	all axial nodes	
3	TZM	W	10	2	
4	TZM	W	10	3	
5	W	W	5	2	
6	W	W	5	3	21
7	W	W	10	2	
8	W	W	10	3	

Common to all cases are the following conditions:

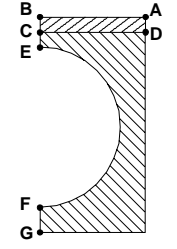
- Helium temperature/pressure at entire channel inner wall 630 °C/8 MPa, assumed HTC=20,000 W/(m<sup>2</sup>K).
- Armour layer thickness 3 mm, castellated and thus ignored for stress assessment.
- Heat load profile according to Figure 4 with separatrix strike point located at y=0.4 m.
- Support points at y=0, y=0.6 m (for 3-point support only), and y=1.6 m provide constraint in z direction.
- Special case 2a has been added to simulate zero deflection in z direction at all axial nodes (plane strain).

#### 3.2.3.1 Temperature distribution

Figure 17 illustrates as example a typical 3-dimensional temperature distribution for load case 1 in one half of the 1.6 m long divertor channel envisaged for the outboard target plate, lined by a 3 mm thick protection layer. The high temperature zone assuming a maximum of 1230 °C is restricted to a small region according to the peaked power profile in y-direction (which in x-direction is uniform). The highest temperature in the structure of 1110 °C occurs at the upper right corner as can be seen in the insert of Figure 17, representing a slice cut at y=0.4 m where temperatures are maximal. The rest of the channel balances at about 630 °C, corresponding to the assumed uniform coolant temperature in this simplified model. Temperatures at other distinct points of the slice are listed in Table 13 for all cases investigated. Of particular interest are points A and D where the peak values occur in the armour and structure, respectively. Also important is point C which is considered as the critical point in stress evaluation. Temperature distributions are very similar for TZM/W and WW combinations, since the thermal conductivity of both materials is similar too. When adopting the operating temperature windows established in section 2.2.1, the table shows that at 10 MW/m<sup>2</sup> peak heat load several points exceed the limits (shaded cells). The tolerable load limit follows from interpolation and will be discussed in section 4.1.1.



**Table 13: Temperatures at distinct points in cross section at  $y=0.4$  m**

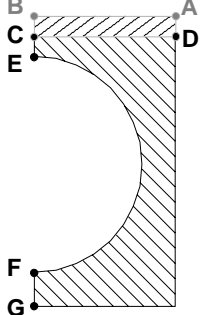
Cases	Temperature ( $^{\circ}\text{C}$ ) at point							Point location
	A	B	C	D	E	F	G	
1, 2 TZM/W, 5 MW/m <sup>2</sup>	1230	1180	1050	1110	919	632	634	
3, 4 TZM/W, 10 MW/m <sup>2</sup>	1830	1730	1470	1600	1210	635	638	
5, 6 W/W, 5 MW/m <sup>2</sup>	1240	1180	1060	1120	920	632	634	
7, 8 W/W, 10 MW/m <sup>2</sup>	1850	1740	1480	1610	1210	635	638	

### 3.2.3.2 Equivalent stress distribution

The stress level in the divertor channel structure is dominated by thermal stresses acting primarily in longitudinal direction with a small contribution from primary stresses caused by the internal pressure. Therefore the fixation of the beam has strong influence. We have studied two types of fixation, i.e., the 2-point support at both ends, 1.6 m apart, allowing free bending and axial expansion, and the 3-point support with an additional support point at  $y=0.6$  m. To illustrate the stress distribution, the equivalent stresses after von Mises are plotted in Figure 18 and Figure 19, respectively for the TZM/W channel. The maximum stress amounts to 313 MPa in the free bending case 1 and to 462 MPa in the 3-point support case 2 at 5 MW/m<sup>2</sup> peak heat flux. They occur close to the edge of the structure, next to point D.

Stress levels at other distinct points of the cross section taken at  $y=0.4$  m are listed in Table 14 for the cases investigated. Of particular interest are points C and D. Stresses in the vicinity of D can be alleviated by cutting the castellation grooves in the armour layer a little deeper into the corners of the channel structure. Therefore, point C is considered here as the critical point in terms of stress limits.

**Table 14: V. Mises equivalent stresses at distinct points in cross section at  $y=0.4$  m**

Case	v. Mises stress (MPa) at point					Point location
	C	D	E	F	G	
1 TZM/W, 5 MW/m <sup>2</sup> , 2-point	204	275	233	69	134	
2 TZM/W, 5 MW/m <sup>2</sup> , 3-point	329	426	281	101	31	
2a TZM/W, 5 MW/m <sup>2</sup> , multiple-point	538	653	395	176	173	
3 TZM/W, 10 MW/m <sup>2</sup> , 2-point	489	604	497	111	284	
4 TZM/W, 10 MW/m <sup>2</sup> , 3-point	725	918	582	197	69	
5 W/W, 5 MW/m <sup>2</sup> , 2-point	237	319	263	73	155	
6 W/W, 5 MW/m <sup>2</sup> , 3-point	384	498	324	114	35	
7 W/W, 10 MW/m <sup>2</sup> , 2-point	512	645	514	121	316	
8 W/W, 10 MW/m <sup>2</sup> , 3-point	792	1020	625	222	76	

Stress levels are similar for TZM/W and W/W combinations, as the direct comparison of cases 2 and 6 in Figure 20 demonstrates, with slightly higher values for the W structure due to the extremely high Young's modulus. The 3-point support produces 50 to 60 % higher stresses at Point C compared to the 2-point support cases, in which the deflections become very large as described next. In the special case of multiple support points, case 2a, stresses

in point C are further increased by 60 % compared to the 3-point support. Some of the stress intensities from Table 14 exceed the limits which will be discussed in section 4.1.2.

### 3.2.3.3 Thermal deformation

We are mainly interested in thermal deformation of the divertor channels in z-direction (for co-ordinates please refer to Figure 17 pp.), as small differences among neighbouring channels can result in considerable leading edge problems. Expansions in y-direction have to be regarded in the design of the manifold. Deformation in x-direction seems to be uncritical due to small dimensions and full symmetry presumed in this work. (This x-symmetry may be destroyed however by leading edge or shadowing effects.)

In Figure 21 is shown, as an example, the thermal deformation in y- and z-direction of a 1.6 m long TZM/W divertor channel supported at 2 and 3 points and loaded with a peak heat flux of 5 MW/m<sup>2</sup> (cases 1 and 2 in Table 12). The maximum thermal deflections in z-direction are of the order +6.5 mm for the 2-point support, and +0.6 mm and -1.4 mm in case of the 3-point support. The expansion in y-direction relative to 20 °C amounts to approximately 6 mm.

Results for the other cases studied are summarised in Table 15. There is an approximately linear dependence from the peak heat load applied. In fact, the positive and negative deflection in the 3-point cases can be balanced by optimising the location of the intermediate support point. On the other hand, the maximum positive deflection coincides almost with the peak of the heat load and is thus the more critical position. In principle, complete suppression of deflection in z-direction could also be considered on the expense of higher stresses as demonstrated with the special case 2a in Table 14.

In summary, the 3-point support seems to be a viable compromise between deflections and stresses. If deflections in z-direction of the order of 1 mm are tolerable, they will not be load limiting in these scenarios as will be shown in section 4.1.

**Table 15: Thermal deformation of divertor cooling channels**

Load case (see also Table 12)	Thermal deformation	
	In z-direction	In y-direction
1, TZM/W, 5 MW/m <sup>2</sup> , 2-point	+6.46 mm at y=0.64 m	5.6 mm
2, TZM/W, 5 MW/m <sup>2</sup> , 3-point	+0.57 mm (-1.42 mm) at y=0.48 m (1.17 m)	5.9 mm
3, TZM/W, 10 MW/m <sup>2</sup> , 2-point	+13.3 mm at y=0.64 m	6.1 mm
4, TZM/W, 10 MW/m <sup>2</sup> , 3-point	+1.05 mm (-2.96 mm) at y=0.48 m (1.17 m)	6.4 mm
5, W/W, 5 MW/m <sup>2</sup> , 2-point	+5.73 mm at y=0.64 m	5.0 mm
6, W/W, 5 MW/m <sup>2</sup> , 3-point	+0.50 mm (-1.25 mm) at y=0.48 m (1.17 m)	5.2 mm
7, W/W, 10 MW/m <sup>2</sup> , 2-point	+11.6 mm at y=0.64 m	5.4 mm
8, W/W, 10 MW/m <sup>2</sup> , 3-point	+0.91 mm (-2.54 mm) at y=0.48 m (1.17 m)	5.7 mm

## Chapter 4 - Performance limits and open issues

The thermal-hydraulics and thermomechanical analyses described in Chapter 3 have indicated a number of dependencies between key operating parameters of a helium-cooled divertor, like heat load, coolant pressure, temperature on one side, and dependent qualifiers like heat transfer, structural temperature, stresses and deformations on the other side. In order to perform this assessment, a divertor concept had to be established in Chapter 2, based on many assumptions in terms of overall configuration, materials, cooling scheme and target plate design, and with the dedicated objective that the concept be viable for future power reactors. In this chapter we concentrate on the performance limits of the proposed design in terms of maximum achievable surface heat flux at the target plates given by materials and design constraints. The limiting criteria adopted in section 4.1 are preliminary and should be regarded as working hypothesis. The potential for improvements or deficiencies within envisaged uncertainties will be addressed qualitatively in section 4.2 before the open issues are summarised in section 4.3.

### 4.1 Performance limits of proposed design

The main features of the proposed helium-cooled divertor of unconventional design, which largely determine its performance limits, are recalled below:

- The concept shall have the potential to efficiently use the divertor power in the power conversion system of future power reactors, calling for high grade heat removal.
- Only a fraction of the divertor power is absorbed by the target plates which are cooled in series with the bulk of the divertor in order to have high coolant inlet temperature.
- The target plates are large components with regions of high thermal flux with unknown profile, extending over 0.6 m to 1 m in poloidal direction on a continuous toroidal belt.
- The target plates are made of refractory materials, requiring operating temperatures of at least 600 °C to minimise neutron irradiation embrittlement.
- The porous media heat exchanger concept shall be used to enhance the heat transfer from the heavily loaded structures to the coolant at acceptable pressure losses.
- The circumferential flow design of the porous wick has been chosen as the only viable configuration that promises to achieve the postulated HTC of 20,000 W/(m<sup>2</sup>K).
- The target plates consist of arrays of parallel poloidal structures with rectangular outer cross section and protection layer (Figure 7), and with coolant collectors at the ends.
- The design is based on scarce and extrapolated data for refractory alloys pertaining to unirradiated conditions as specified in section 2.2.2.

The divertor channel design and analysis focused on two material options (the TZM/W and the W/W combination) and two fixation variants (the 2-point support and the 3-point support) which are evaluated in terms of their maximum allowable heat flux against the design criteria listed below. The results are summarised in Table 16 and explained in the paragraphs to follow.

- Maximum allowable temperature at any point of the W protection layer is 1800 °C.
- Maximum allowable temperature at any point of the W structure is 1400 °C.
- Maximum allowable temperature at any point of the TZM structure is 1200 °C.
- Equivalent v. Mises stress at point C of the structure (compare Table 14) not greater than 3Sm(T) as specified in Table 7 for TZM or W alloys, respectively.
- Channel thermal out-of-plane deflection not greater than 1 mm.

#### 4.1.1 Heat flux limits set by temperatures

In Figure 22 is plotted the temperature at distinct points of the TZM/W divertor channel in the cross section of maximum heat flux as function of peak heat flux as presented in section 3.2.3.1. The dependency is practically linear, with the hottest point being point A at the edge of the tungsten armour, followed by point B in the centre of the heated surface. The curve pertaining to point A intersects the allowable temperature of 1800 °C for tungsten alloy at a heat flux of 9.7 MW/m<sup>2</sup>, which is thus the performance limit relative to this particular criterion. Likewise we look at the TZM structure with point D running hottest. The curve of point D intersects the allowable temperature of 1200 °C for TZM at the heat flux of 5.9 MW/m<sup>2</sup>, which is more stringent than the armour temperature criterion. In other words, there is large margin in the armour thickness (assumed here as 3 mm) before the temperature criterion at a heat flux of 5.9 MW/m<sup>2</sup> will be reached, namely additional 7 mm. This assessment does not depend on the type of channel fixation or on the poloidal heat flux profile, but it does depend on the boundary conditions applied in the analysis with regard to coolant temperature and heat transfer coefficient.

In a similar way the performance limits were found for the W-alloy/W (or in short W/W) combination with reference to Figure 23, leading to 9.5 MW/m<sup>2</sup> when applying the armour temperature criterion and to 7.8 MW/m<sup>2</sup> set by the 1400 °C temperature limit for the tungsten alloy structure. These heat flux limits are entered into the summary Table 16 on page 29, but other criteria need to be tested as follows.

#### 4.1.2 Heat flux limits set by stresses

In Figure 24 is plotted the equivalent stress after v. Mises at distinct points of the TZM/W divertor channel structure in the cross section of maximum stresses (which coincides with the location of maximum heat flux) as function of peak heat flux as presented in section 3.2.3.2. The curves were obtained for the 3-point support. The dependency is almost linear, with the highest stresses occurring in point D (or close to it as mentioned earlier) at the edge of the TZM structure, followed by point C at the line of symmetry. It was pointed out in the analysis that stresses in point D and its vicinity can be alleviated by design measures and, therefore, point C is considered as the critical one. The stress limit for point C is given by the condition  $S_c < 3S_m$  ( $S_c = v.$  Mises stress intensity at point C,  $3S_m = 3S_m(T_c) = \text{allowable stress intensity as function of temperature in point C}$ ). Having defined  $3S_m(T_c)$  in Table 7 and computed  $T_c(\hat{q})$  (with  $\hat{q} = \text{peak heat flux}$ ) according to Figure 22, we can plot  $3S_m(\hat{q})$  in Figure 24 as dashed line and find the intersection at the heat flux of 5.5 MW/m<sup>2</sup>. In the same way the heat flux limit for the W/W divertor with 3-point support is evaluated as 4.6 MW/m<sup>2</sup> from Figure 25.

For the 2-point support the situation is similar, however stress levels are much lower as already shown in Table 14. The same procedure as for the 3-point support leads to the heat flux limit of 6.6 MW/m<sup>2</sup> for the TZM/W divertor channel and to 6.5 MW/m<sup>2</sup> for the W/W channel. Also in this case the stress criterion is reached in point C, although the stresses in point E are a little higher, but at reduced temperatures which overcompensates the stress effect.

#### 4.1.3 Heat flux limits set by deflections

In Figure 26 is plotted the extreme of the thermal deflection of the TZM/W divertor channel as function of peak heat flux as presented in section 3.2.3.3. The curves were obtained for the 2-point and 3-point support. For the latter we have two extreme values, one positive and one negative as the deflection line in Figure 21 illustrates. It is seen that the transverse deflection in the 2-point support case is very large and the tolerable limit of 1 mm would be reached at a peak heat flux of less than 1 MW/m<sup>2</sup>. Even if the position of the support points was optimised by placing them away from the ends, a factor of about two could be gained only. Thus the 2-point support with the lower stress level is not acceptable for large components.

For the 3-point support assumed in this analysis with the intermediate support point at  $y=0.6$  m the deflection criterion would be violated at peak heat fluxes  $>3.5$  MW/m<sup>2</sup> by the backward deflection (denoted as ‘3-point minus’ in Figure 26), whereas the deflection in the heavily heated region at  $y=0.48$  m (denoted as ‘3-point plus’) allows a peak heat flux of about 10 MW/m<sup>2</sup>. By trimming the intermediate support point so that the positive and negative deformation would be of equal magnitude, the heat flux limit would be reached at approximately 6 MW/m<sup>2</sup>.

The W/W divertor channel shows a similar deflection behaviour as the TZM/W, which is not discussed here in detail.

#### 4.1.4 Summary of performance limits

The thermomechanical analysis focused on exploring the tolerable heat flux at the divertor plate with respect to temperature, stress and deflection limits. As mechanical constraints a 2-point support and a 3-point support of the 1.6 m long channels have been investigated. The results are listed in Table 16 for the two variants of structural materials and the conditions specified in the analysis section 3.2. From each column in Table 16 the smallest heat flux value must be taken as the tolerable limit (shaded cells). It is obvious that the 2-point support must be ruled out because of excessive deflection. Then for the 3-point support the v. Mises criterion is the most stringent one, leading to tolerable heat loads of approximately 5.5 and 4.6 MW/m<sup>2</sup> for the TZM and W option, respectively. The armour thickness can be increased by several mm before it becomes a limiting factor, because it affects only the maximum temperature but not (due to the castellation) the stresses. The sensitivity of the performance limit to several parameters is presented in the next section.

**Table 16: Heat flux limits in MW/m<sup>2</sup> for target plates made from TZM and W alloy**

Structural material (combined with tungsten armour)	TZM/W		W/W	
	2-point	3-point	2-point	3-point
Type of mechanical support of 1.6 m long channels				
Temperature criterion (1400 °C for W, 1200 °C for TZM)	5.9	5.9	7.8	7.8
Temperature criterion (1800 °C for tungsten armour)	9.7	9.7	9.5	9.5
v. Mises stress criterion (3Sm limit)	6.6	5.5	6.5	4.6
Deflection criterion (1 mm transverse)	1-2	≅6	1-2	≅6

#### 4.2 Potential for improvements

The most sensitive parameters or effects with respect to the performance limits in this study turned out to be

- The 3Sm(T) characteristics of the structural material (Table 7)
- The heat transfer coefficient that affects the temperature level (section 2.3.1)
- The coolant temperature affecting the temperature level at critical points (Table 9)
- The channel wall thickness (along the line C-E in Table 14)
- The thermomechanical model adopted in the analysis (section 3.1)

A brief sensitivity study has been performed to indicate the impact of the parameters mentioned above on the performance limits. This assessment was made for the best performing variant, i.e., the TZM/W cooling channel with 3-point support. The results are summarised below and visualised in Figure 27.

The *allowable stress limit*, 3Sm(T), is in fact very uncertain for the refractory materials involved. It depends, among others, on the fabrication process, component size and heat treatment, and may also be altered by neutron irradiation. Thus, establishing the material

data base would be a prime issue when pursuing helium-cooled divertors suitable for high-grade heat extraction. The plot at the upper left in Figure 27 shows the influence of a postulated change in the 3Sm limit on the gain or loss in heat flux limit for the load case 2 from Table 12. For instance, if the 3Sm limit can be improved by 20 % (i.e., applying a multiplication factor of 1.2 on the 3Sm values from Table 7) the performance limit of the TZM/W divertor goes up by 8 %, from 5.5 to 6 MW/m<sup>2</sup>.

The *achievable heat transfer coefficient* (HTC) was postulated to be 20,000 W/(m<sup>2</sup>K) for the porous media design, which seems to be an optimistic assumption (compare section 2.3.1.3). The impact of HTC on the performance limit is twofold. Firstly, it affects the temperature level at the critical point, C, and secondly, it influences the temperature gradient (and hence the thermal stress) across the channel height. To evaluate both effect two extra calculations with the HTC as parameter have been performed, namely with HTC=15,000 W/(m<sup>2</sup>K) and 25,000 W/(m<sup>2</sup>K). The resulting change in heat flux limit by reaching the 3Sm criterion is shown in Figure 27, lower left frame. For instance, improving the HTC by 25 % from 20,000 to 25,000 W/(m<sup>2</sup>K) would gain almost 10 % in performance limit (from 5.5 to 6 MW/m<sup>2</sup>) for the TZM/W divertor channel with 3-point support. On the other side, the losses would be even larger if the HTC=20,000 W/(m<sup>2</sup>K) would not be attained.

The *temperature level* of the divertor structure is determined to a large extent by the coolant inlet temperature to the target plate assumed as 632 °C. This was chosen with regard to the operating temperature window of the refractory materials defined in section 2.2.1 with the lower boundary assumed as 600 °C. Thus, there is a nominal margin to lower the inlet temperature by 32 °C and thereby shift the calculated temperature level in the whole divertor channel by the same amount. The equivalent stress distribution for given peak heat fluxes would practically be unaffected by this measure, but the 3Sm limit would be reached only at higher peak heat fluxes. The change in heat flux limit (performance limit) as result of a shift in the temperature level, while keeping everything else unchanged, is illustrated in Figure 27, upper right. For instance, reducing the temperature level in the TZM/W divertor channel with 3-point support by 50 °C would gain 4.2 % in performance limit, i.e., 5.73 MW/m<sup>2</sup> instead of 5.5 MW/m<sup>2</sup>.

Optimisation of the *channel cross section*, for example by reducing the wall thickness between points C-E, could help to reduce temperatures and thermal stresses, although primary stresses would go up. An estimate revealed the sensitivity of the heat flux limit by changing the channel thickness by ±1 mm as indicated in Figure 27, bottom right. For example, reducing the wall thickness from 3 mm to 2 mm would gain 8 % in performance limit, i.e., the heat flux limit goes up from 5.5 to 5.9 MW/m<sup>2</sup>.

As outlined in the *thermomechanical model* description in section 3.1.3, the stress analysis presumes constant coolant temperature throughout the channel inner wall as boundary condition. This is a strong simplification. In fact, the coolant temperature increases along its flow path by a nominal mean  $\Delta T=168$  K and locally even much more, depending on the axial heat flux profile (section 3.2.2.2). Hence, the channel wall sees a complex axial and circumferential coolant temperature distribution which changes the thermal stress distribution as well. With regard to the temperature at the stress-critical point, C, the model adopted applies quite well, since the coolant at the opposite point, E, impinges with the inlet temperature as assumed. Subsequently, on its split path through the wick, the coolant picks up heat very fast and carries heat to the back of the channel structure. This effect tends to equalise the temperature distribution in a given cross section and thus reduces thermal stresses in C. Consequently, the analysis seems to be conservative with respect to the stress criterion in point C, but it definitely underestimates peak temperatures in point D. A quantitative assessment of this cross flow effect on performance limit would need refined models.

In *summary*, one can see a small potential for improving the performance limit set by the stress criterion up to 10 % by individual measures discussed here, i.e., from 5.5 to 6 MW/m<sup>2</sup> for the TZM/W channel with 3-point support. Superposition is not allowed without questioning

the other criteria, which also become effective at a peak heat flux of about 6 MW/m<sup>2</sup> as shown in Table 16.

### **4.3 Open issues and required R&D**

The achievable heat transfer coefficient of porous media, made of refractory materials in order to stand the high temperature, needs experimental proof with helium cooling. The value assumed in this study seems to be realistic, but the potential for improvements is judged to be small.

Uncertainties in the assessment are further induced by the mechanical properties of the structural materials. The data used are derived from stress relieved condition, unirradiated. Effects of irradiation, fabrication, alloying, component size, recrystallisation and stress concentration are largely unknown. They may, in part, compensate each other. Hence, the main issue is seen in lifetime performance rather than conventional thermomechanical layout (see below).

Fabrication techniques for porous media heat exchangers with refractory alloys are in the early stage of development. In particular, reliable bonding of the porous media in form of bonded particles or 'foam' with the heated structure is essential and needs to be demonstrated. Detachment can perhaps lead to unstable overheating and early failure.

The porous media concept with circumferential flow has limited design flexibility against varying heat flux profiles, especially for large heated lengths and substantial power peaking. Tailoring the cross sections in longitudinal direction could help but would complicate fabrication.

Combined thermal-hydraulic modelling of the cooling channel should be employed in order to make use of the circumferential heat transport that tends to equilibrate temperature and thermal stresses in the structure.

### **4.4 Comments on lifetime, maintainability, reliability**

Divertor lifetime cannot be assessed at present. The goal must be a few years of full power operation with up to about 1000 operational thermal cycles during lifetime. There are a number of life-limiting factors that have to be explored in the long run and are basically related to the material behaviour. (1) Embrittlement of the structural material during irradiation has been accounted for to some extent, according to present knowledge, by choosing operational temperatures above 600-700 °C. (2) Low cycle fatigue may become a problem at the castellation grooves and at the numerous joints and manifolds. (3) Swelling, although relatively small, is certainly an important factor in the overall design with regard to joints, supports, differential effects, for which the data base is not available. (4) Erosion of the W armour is expected to be small in detached plasma operation and should not be life limiting, unless there are unexpected plasma instabilities. (5) Wall/coolant interaction is generally no corrosion concern with helium, however oxygen impurities in the coolant in combination with W and Mo structure needs attention. (6) Activation has also not been quantified but is a waste disposal and maintenance issue rather than a lifetime problem. (7) The decay heat and its medium term removal need to be assessed in cases of cooling disturbance. A few further design specific factors that can impede the lifetime are mentioned: (8) leak tightness, (9) stability of porous media/structure thermal contact, (10) plugging of the porous media requiring good filtering, and (11) durability of instrumentation and control equipment.

Maintainability of the divertor depends on the overall plant maintenance. From the viewpoint of divertor engineering the cassette type (e.g., 1/48 segment) with radial and radial-toroidal (for hidden cassettes) motion for replacement through horizontal ports is preferred. The sizeable coolant pipes of at least 4 pipes per cassette with inner diameter of about 100 mm may raise space problems in the port region. Please note that supply lines for 3 cassettes must be accommodated per port. In-situ repair of divertor components will be very limited.

Instead, complete cassette replacement and hot cell repair should be envisaged in case of damage or malfunction.

Nothing can be said about reliability because of the frontier nature of the task in terms of complex structure, new techniques, unknown material properties and unclear loading conditions from plasma physics.



## Chapter 5 – Summary and Conclusions

### 5.1 Summary

High Heat Flux Components (HHFC) developed in the past focused on water cooling with heat loads up to  $30 \text{ MW/m}^2$ . They were based on copper alloys with exceptionally high thermal conductivity. This implied that the maximum temperature in the coolant confining structure had to be kept low making the system unattractive for power conversion. The present aim in the frame of the European Programme “Preparation of a Power Plant conceptual Study, Plant Availability, PPA” is to exploit helium cooling, featuring high-grade heat production, compatibility with helium-cooled blanket systems and avoiding chemical reaction hazards. This calls for elevated coolant temperature and the use of refractory alloys as structural materials. Thus, the objective of this task is to explore the manageable heat flux limits of helium-cooled divertor concepts that employ high temperature resistant materials with high thermal conductivity, good wall-to-coolant heat transfer characteristics and adequate coolant parameters.

This report starts with an overview of the main design constraints or assumptions in terms of general divertor configuration, dimensions, operating conditions, material choice, and other features, which give the rationale for the concept investigated as described in Chapter 2. This concept is regarded as a viable and representative solution for the given set of constraints, where many details have still to be worked out. The type, volume and results of the analysis performed for the proposed divertor design are described in Chapter 3, which lead to the performance limits summarised in Chapter 4. Here, also the deficiencies and open issues are addressed. Conclusions are drawn at the end of Chapter 5.

The *overall divertor design considerations* started from the PPA plant parameters. Given the total fusion power of 3607 MW, the divertor has to be designed for a total power to divertor of 670 MW, leading to a linear power at the target plates of 3 MW/m of toroidal length. With assumed heat flux profiles as working hypothesis, the corresponding peak heat fluxes would be  $5 \text{ MW/m}^2$  in case of a flat power profile and  $9.2 \text{ MW/m}^2$  for the peaked profile. Uncertainties result further from unknown divertor performance with view to power sharing between inboard and outboard, and between divertor sub-components. The ITER divertor concept as of 1998 has been used as typical model in this assessment.

A review of *potential divertor materials* led to the conclusion, that tungsten or tungsten alloys are to be used as armour material. Consequently, tungsten (or tungsten alloys) and molybdenum (or molybdenum alloys) are the only viable options as structural materials for target plates. For these materials the following operating temperature windows are considered acceptable in this work: Tungsten or tungsten alloy as armour material  $600 \text{ }^\circ\text{C} - 1800 \text{ }^\circ\text{C}$ , tungsten or tungsten alloy as structural material  $600 \text{ }^\circ\text{C} - 1400 \text{ }^\circ\text{C}$ , molybdenum or molybdenum alloy as structural material  $600 \text{ }^\circ\text{C} - 1200 \text{ }^\circ\text{C}$ . The bulk of the divertor is assumed to be fabricated of ferritic martensitic steel with an operating temperature window of  $250 \text{ }^\circ\text{C} - 650 \text{ }^\circ\text{C}$ .

*Heat transfer enhancement methods* for helium cooling are reviewed. Attractive heat transfer coefficients of 15,000 up to 50,000  $\text{W}/(\text{m}^2\text{K})$  appear to be achievable in principle. Most of the methods, however, are not well suited for large surfaces as needed in divertor application, or require complicated manifolding systems. This is particularly true for micro-channels, honeycombs, and jet impingement. Uncertainties arise from the fact that satisfactory results have been reported in the literature so far only for low temperature systems with high conductive materials like copper or aluminum. The performance of heat exchangers made of refractory materials needs to be proved with view to their different physical properties, fabricability, bonding techniques and durability. The best potential for divertor application among these unconventional systems is seen in the porous media concept or in the micro-channel/micro-fin concept with expected heat transfer coefficients of about 20,000  $\text{W}/(\text{m}^2\text{K})$ . The porous media concept has been chosen in this study.

The overall design considerations led to the following *conceptual design*. The divertor target plates are envisaged to be slightly bent structures, following the contour of the cross section of the PPA divertor cassette. Thus they measure typically 1.6 m x 1.16 m at the outboard. These plates are assumed to consist of arrays of separate poloidal channels, being supported at the ends and at intermediate supports. Channel ends are connected to manifolds to provide inlet and outlet terminals for the helium coolant. Only small out-of-plane deflections can be tolerated. To this end the target plate design concentrates on a single channel with a typical cross section of 36 mm x 39 mm and a 28 mm diameter bore over the entire channel length to accommodate the porous media insert. These consist of the wick and two staggered and slit coolant tubes for helium inlet and outlet, known as the circumferential flow type design. The whole insert extends across the heavily loaded channel part only, i.e., approximately 0.6 m.

The *analysis of the proposed concept* comprises three fields: (i) The overall divertor cooling parameters being responsible for the integration of the divertor cooling system into the plant power conversion concept, (ii) 1D thermal-hydraulics analysis of the target plates as the critical divertor components that drive main cooling parameters and hence, boundary conditions for the thermomechanics, (iii) 3D thermomechanical elastic analysis of the target plate in terms of stress and strains as dominating performance limit.

The *thermal-hydraulic analysis results* are summarised as follows. Based on first assumptions for divertor configuration, coolant flow scheme, target plate design, and materials temperature windows, the following reference values are chosen from the parametric study: Helium is routed in series at first through the bulk of the divertor at inlet/outlet temperature of 400 °C/632 °C and subsequently through the target plates at inlet/outlet temperature of 632 °C/800 °C. The inlet pressure is 8 MPa. The pumping power can be kept at an acceptable level, but there is little freedom to alter the helium temperatures under the restrictions assumed. The coolant parameters are suited for an effective power conversion in a self-contained conversion system. The porous media wick dimensions have been optimised with regard to pressure drop and heat transfer for a certain design point. However, large deviations from nominal thermal-hydraulic conditions make the layout ineffective as will be the case for strongly peaked power profiles.

The *thermomechanical analysis* focused on exploring the tolerable heat flux at the divertor plate with respect to temperature, stress and deflection limits. As mechanical constraints a 2-point support and a 3-point support of the 1.6 m long channels have been investigated. The results show that the 2-point support must be ruled out because of excessive deflection. For the 3-point support the v. Mises criterion is the most stringent one, leading to tolerable heat loads of approximately 5.5 and 4.6 MW/m<sup>2</sup> for the TZM/W and W/W material combinations, respectively. The W armour thickness can be increased from 3 mm by several mm before the peak temperature becomes a limiting factor. The sensitivity analysis with respect to the performance limits yielded the following parameters as the most important ones: the 3Sm(T) characteristics of the structural material, the heat transfer coefficient, the coolant temperature, the channel wall thickness, and the thermomechanical model adopted in the analysis. One can see a potential for improving the performance limit set by the stress criterion up to 10 % by individual measures, i.e., from 5.5 to 6 MW/m<sup>2</sup> for the TZM/W channel with 3-point support. Temperature and deflection criteria become effective at this peak heat flux as well.

## 5.2 Conclusions

Analysis of the porous media heat exchanger concept for application in high heat flux design has shown that peak heat fluxes of 5.5 to 6 MW/m<sup>2</sup> are feasible with unconventional, helium-cooled divertor concepts, given that the operating temperature in the only structural materials deemed viable (molybdenum and tungsten alloys) must not fall below 600-700 °C for reasons of embrittlement. Heat flux limits are given by stress criteria in a 3-point supported structure, but also temperature criteria and deflection criteria have to be observed. A 2-point support causing substantially lower stresses would lead to excessive deflection. The potential for further improvements through better heat transfer, material characteristics and design optimisation are marginal when compared to uncertainties in specifying the required heat load at the divertor plates. Coolant parameters can be kept in an attractive range for power conversion, e.g., inlet/outlet temperature of 400 °C/800 °C at 8 MPa, allowing an extra electric output of between 200 and 325 MW<sub>el</sub> (at 3607 MW fusion power), depending on the plant power conversion concept. In general, it must be noted, that peak heat fluxes of this magnitude are most likely not sufficient for a power reactor. With present assumptions on dimensions, power to target plates and poloidal power peaking profile, the power capacity is only 2/3 of what would be needed.

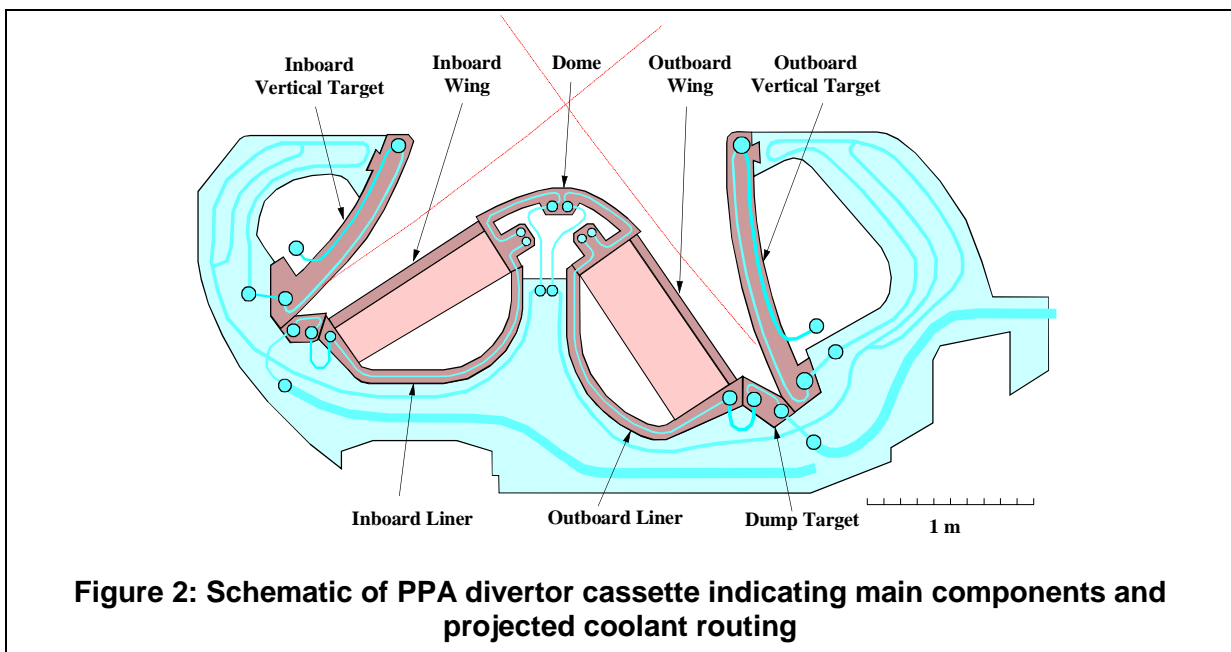
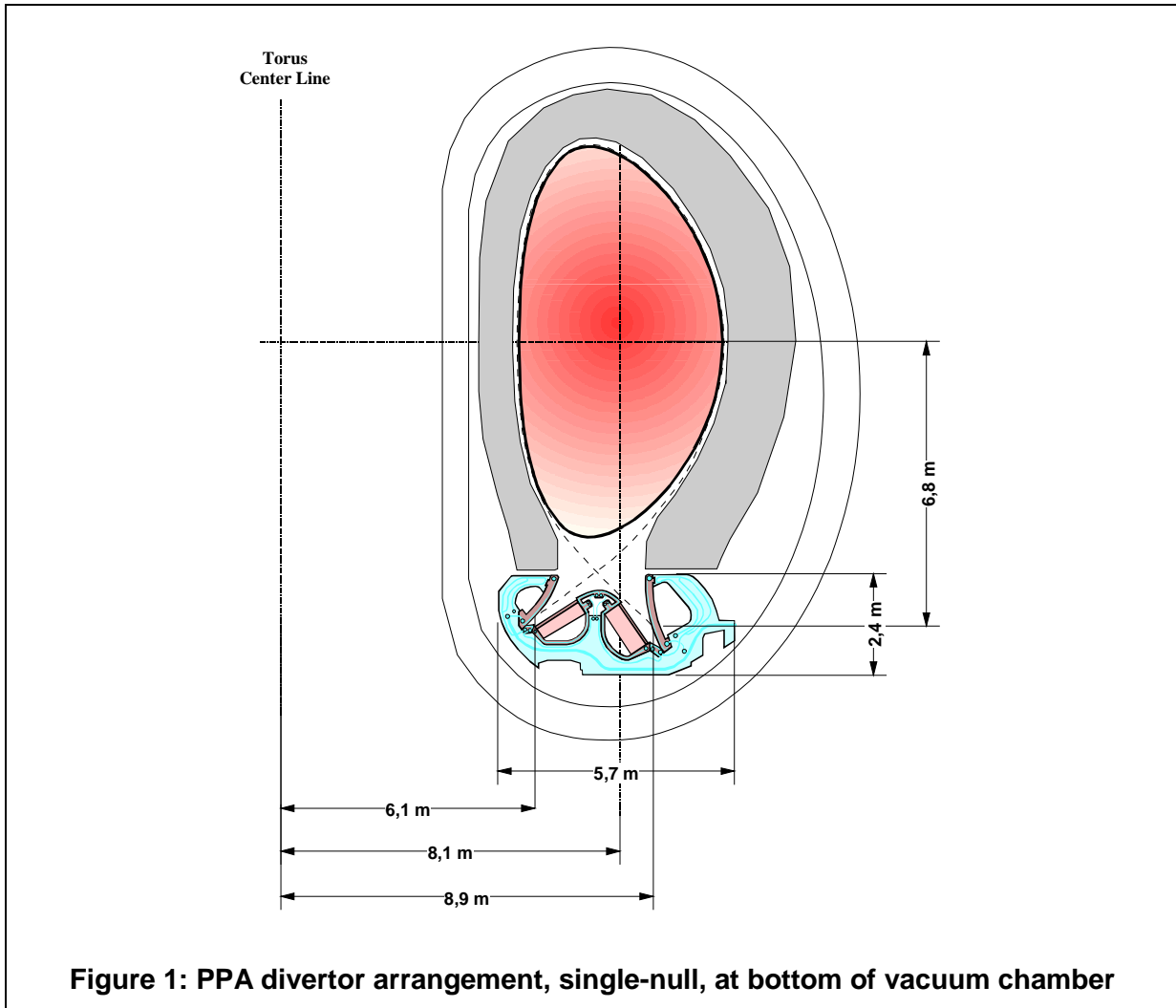
Besides the power capacity other issues need to be addressed in a reactor study. The achievable heat transfer coefficient of porous media, made of refractory materials in order to stand the high temperature, needs experimental proof. The value assumed in this study seems to be realistic, but the potential for improvements is judged to be small. Uncertainties in the assessment are further induced by the mechanical properties of the structural materials. The data base is very incomplete. The data used are derived from stress relieved condition, unirradiated. Effects of irradiation, creep, fabrication, alloying, component size, recrystallisation and stress concentration are largely unknown, but may, in part, compensate each other. Hence, the main issue is seen in lifetime performance rather than conventional thermomechanical layout. Fabrication techniques for porous media heat exchangers with refractory alloys are in the early stage of development. In particular, reliable bonding of the porous media in form of bonded particles or 'foam' with the heated structure is essential and needs to be demonstrated. Detachment can perhaps lead to unstable overheating and early failure. The porous media concept with circumferential flow has limited design flexibility against varying heat flux profiles, especially for large heated length and substantial power peaking. Tailoring the cross sections in longitudinal direction could help but would complicate fabrication. Nothing can be said about reliability because of the frontier nature of the task in terms of complex structure, new techniques, unknown material properties and unclear loading conditions from plasma physics.

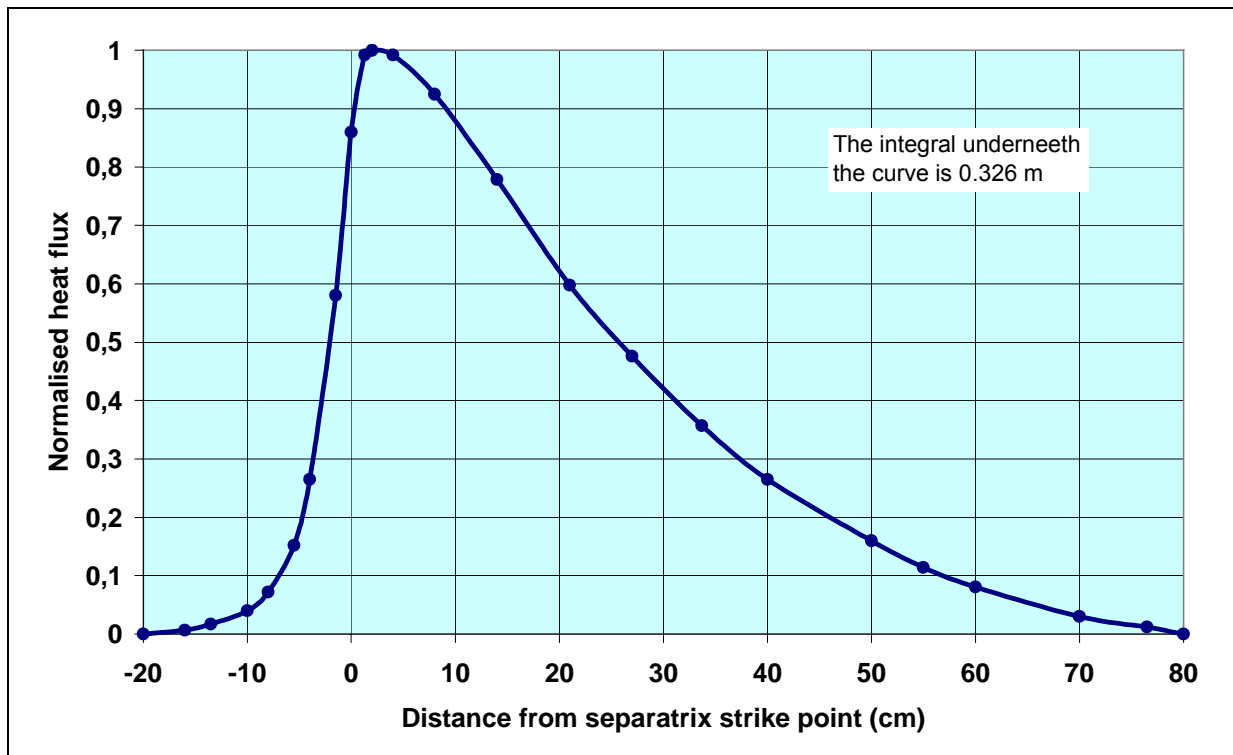
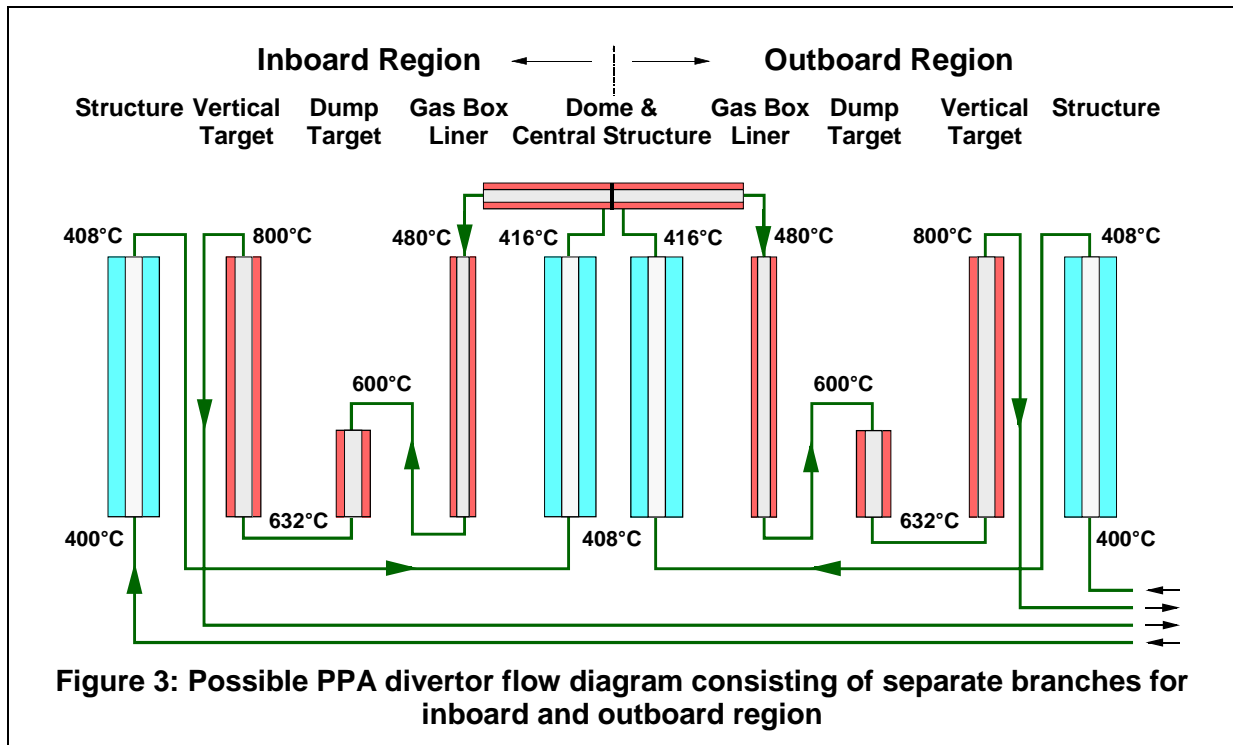


## References

- [1] J. Schlosser, J. Boscari: Thermal-hydraulic tests at NET/ITER relevant conditions on divertor targets using swirl tubes, Proc. 6th International Topical Meeting on Nuclear Reactor Thermal Hydraulics, Grenoble, France, October 5-8, 1993, 815-824.
- [2] D. Bolsch: Thermohydraulische Auslegung von gasgekühlten hochbelasteten Komponenten in Fusionsreaktoren, Diplomarbeit am Institut für Reaktortechnik, Universität Karlsruhe (TH), 1986.
- [3] M. Merola, R. Matera: Optimisation of the monoblock divertor plate by the use of ultrahigh thermal conductivity carbon fibres, Commission of the European Communities, EUR 13594 EN, 1991.
- [4] R.D. Boyd: Heat transfer for fusion component application, Fusion Technology Vol. 13, May 1988, 644-653.
- [5] E. Zolti: Extensions of the code IAFETIN, The NET Team, Internal Note N/I/3300/9/A, Feb. 1991.
- [6] A. Soria, V. Renda, L. Papa: Thermal analysis of a tokamak divertor plate after a sudden coolant dry-out, submitted to Fus. Eng. Des. about 1990.
- [7] C.B. Baxi: Evaluation of helium cooling for fusion divertors, Fus. Eng. Des. 25, 1994, 263-271.
- [8] J.E. Lindemuth, D.M. Johnson, J.H. Rosenfeld: Evaluation of porous metal heat exchangers for high heat flux components, ASME Winter Annual Meeting 1994.
- [9] J.H. Rosenfeld, J.E. Lindemuth, M.T. North: Evaluation of porous media heat exchangers for fusion application, Fusion Technology Vol. 29, July 1996, 449-458.
- [10] E.K. Kalinin, G.A. Dreister, N.V. Paramonov et.al.: Comprehensive study of heat transfer enhancement in tubular heat exchangers, Experimental Thermal and Fluid Science 1991; 4:656-666.
- [11] International Thermonuclear Experimental Reactor, Final design report G 17 DDD 5 98-05-29 W0.2, 1998.
- [12] I. Cook, P. Knight, N. Taylor, D. Ward: Definition and parameters for initial blanket and divertor studies, PPA/3.1/UKAEA/2, March 1999.
- [13] M.C. Billone: Summary of materials advances session, Snowmass Chamber Science & Technology, Session CQ7, July 15-16, 1999.
- [14] Plansee Aktiengesellschaft: Tungsten product specification, 39.39.50-GR130, 1997.
- [15] Plansee Aktiengesellschaft: A high-temperature molybdenum alloy, Brochure.
- [16] E. Zolti: Material data for predesign analysis of in-vessel components, The NET Team, Internal Note N/I/3300/5/A, Apr. 1990.
- [17] O.G. Martynenko: Heat and mass transfer bibliography - CIS works, Int. Jour. of Heat Mass Transfer Vol. 40, No. 1, 1-14, 1997.
- [18] E.R.G. Eckert, R.J. Goldstein, W.E. Ibele et.al.: Heat transfer - a review of 1995 literature, Int. Jour. of Heat and Mass Transfer 42 (1999) 2717-2797.
- [19] J.P. Tsia, J.J. Hwang: Measurements of heat transfer and fluid flow in a rectangular duct with alternating attached-detached rib-arrays, Int. Jour. of Heat and Mass Transfer 42 (1999) 2071-2083.
- [20] P. Dutta, S. Dutta: Effect of baffle size, perforation, and orientation on internal heat transfer enhancement, Int. Jour. of Heat and Mass Transfer 41 (1998) 3005-3013.

- [21] T.A. Ruch, T.A. Newell, A.M. Jacobi: An experimental study of flow and heat transfer in sinusoidal wavy passages, *Int. Jour. of Heat and Mass Transfer* 42 (1999) 1541-1553.
- [22] R. P. Saini, J. S. Saini: Heat transfer and friction factor correlations for artificially roughened ducts with expanded metal mesh as roughness element, *Int. Jour. of Heat Mass Transfer*, Vol. 40, No. 4, 973-986, 1997.
- [23] C.P.C. Wong, R.E. Nygren, C.B. Baxi et.al.: Helium-cooled refractory alloys first wall and blanket evaluation, 5th ISFNT, Sep. 19-24, 1999, Roma, Italy.
- [24] VDI-Wärmeatlas, Berechnungsblätter für den Wärmeübergang, 4. Auflage 1984.
- [25] S. Chikh, A. Boumediene, K. Bouhadeif, G. Lauriat: Analysis of fluid flow and heat transfer in a channel with intermittent heated porous blocks, *Heat and Mass Transfer* 33 (1998) 405-413.
- [26] Saddleback Aerospace: Copper micro-impingement coolers, <http://www.saddle-aero.com>, Nov 1999.
- [27] D.-Y. Lee, K. Vafai: Comparative analysis of jet impingement and microchannel cooling for high heat flux application, *Int. Jour. of Heat and Mass Transfer* 42 (1999) 1555-1568.
- [28] T.J. Lu: Heat transfer efficiency of metal honeycombs, *Int. Jour. of Heat and Mass Transfer* 42 (1999) 2031-2040.
- [29] J.-J. Hwang, C.-C. Lui: Detailed heat transfer characteristic comparison in straight and 90-Deg. turned trapezoidal ducts with pin-fin arrays, *Int. Journal of Heat and Mass Transfer* 42 (1999) 4005-4016.
- [30] C.B. Baxi, C.P.C. Wong: Review of helium cooling for fusion reactor application, *International Symposium on Fusion Nuclear Technology* 5, Sep. 1999, Rome, I.
- [31] R. Gordon, J. Cobonque: Heat transfer between a flat plate and jets of air impinging on it, *International Developments in Heat Transfer*, p. 454.
- [32] SPEAKEASY Manual, Speakeasy Computing Corporation, 222 west Adams street, Chicago, Illinois 60606.
- [33] S. Hermsmeyer et al.: Improved helium cooled pebble bed blanket – Final Report of PPA Preparatory Study, Task PPA2.3, FZKA-6399.







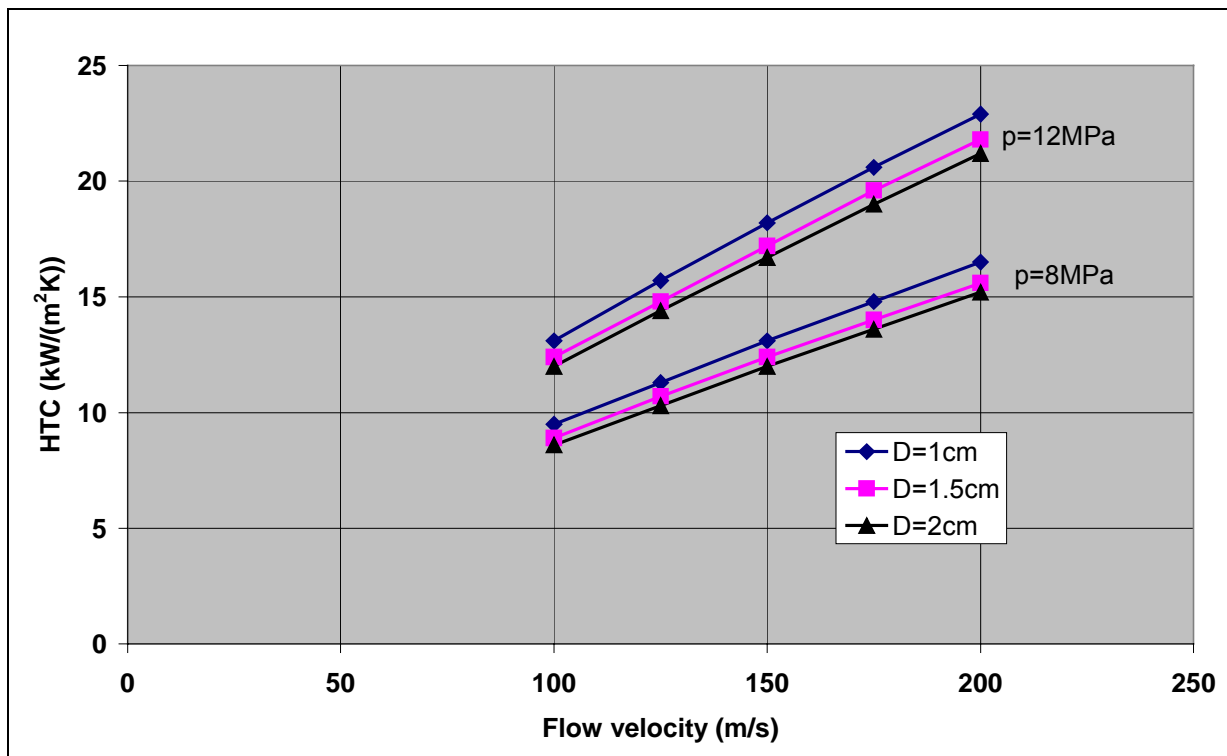


Figure 5: Heat transfer coefficient in smooth tubes for different inner diameters, D, and helium pressures, p

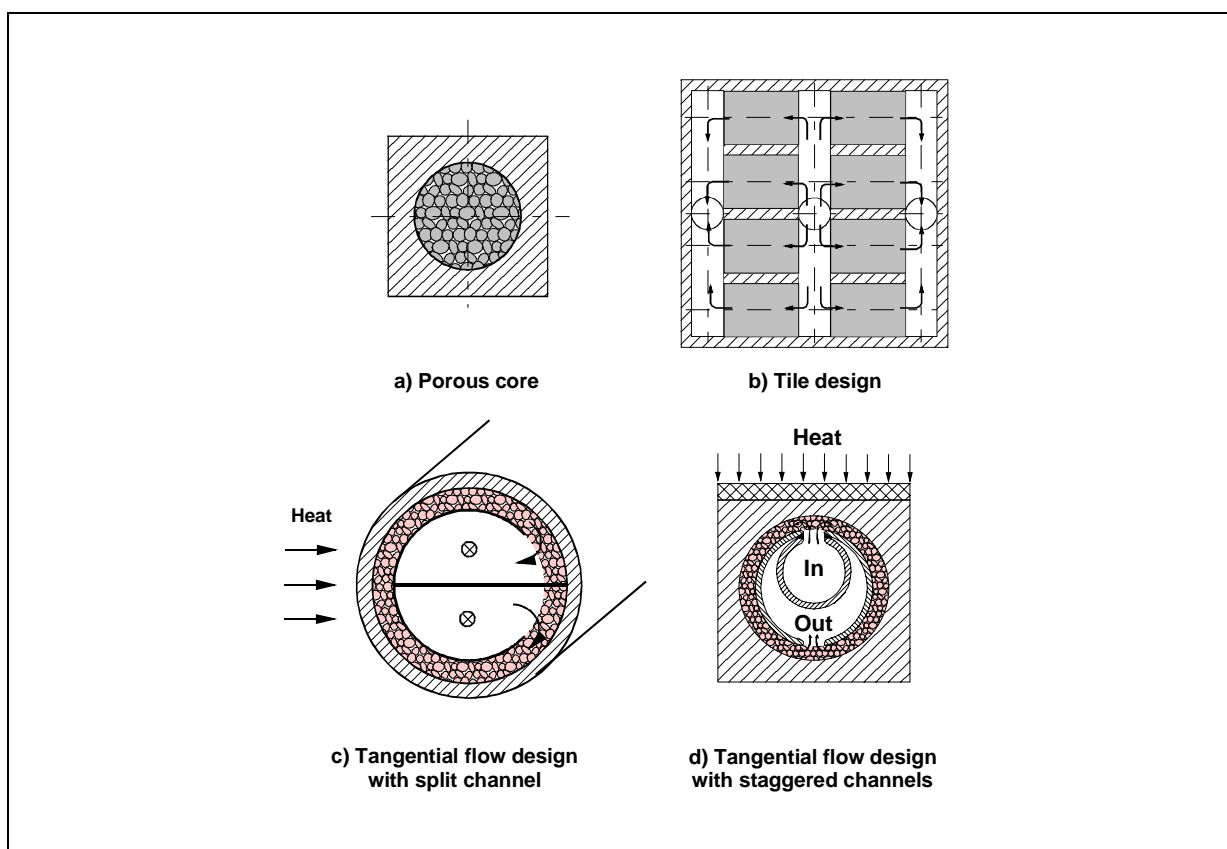


Figure 6: Evolution of porous media heat exchanger design

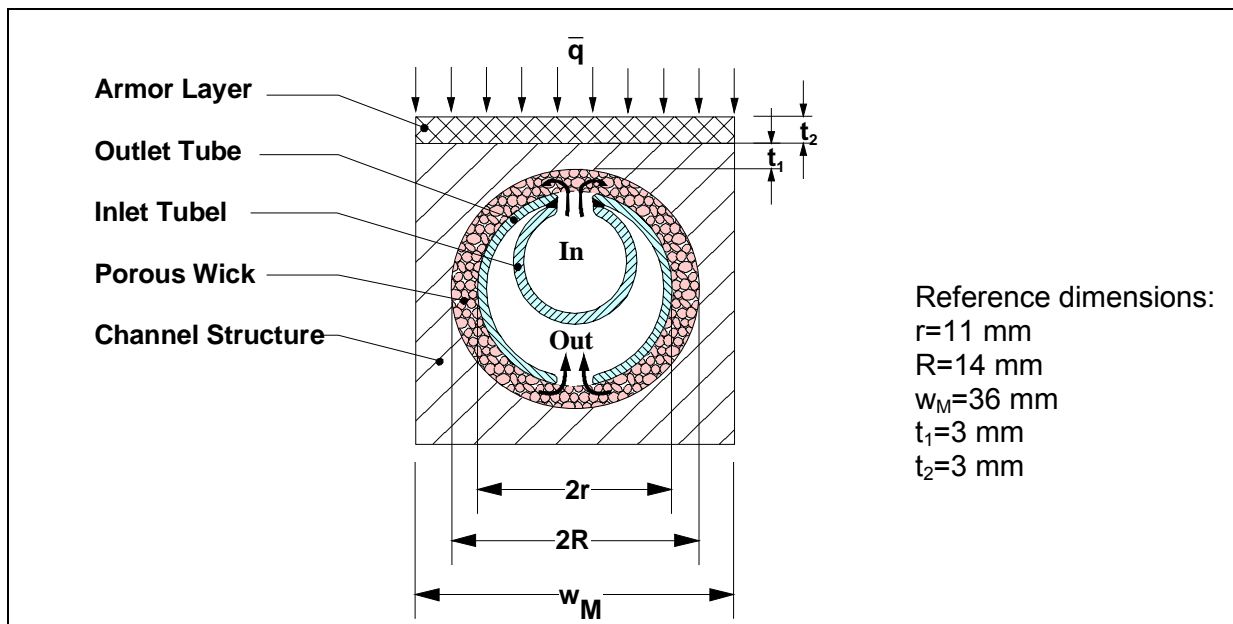


Figure 7: Typical cross section of a porous media target plate channel

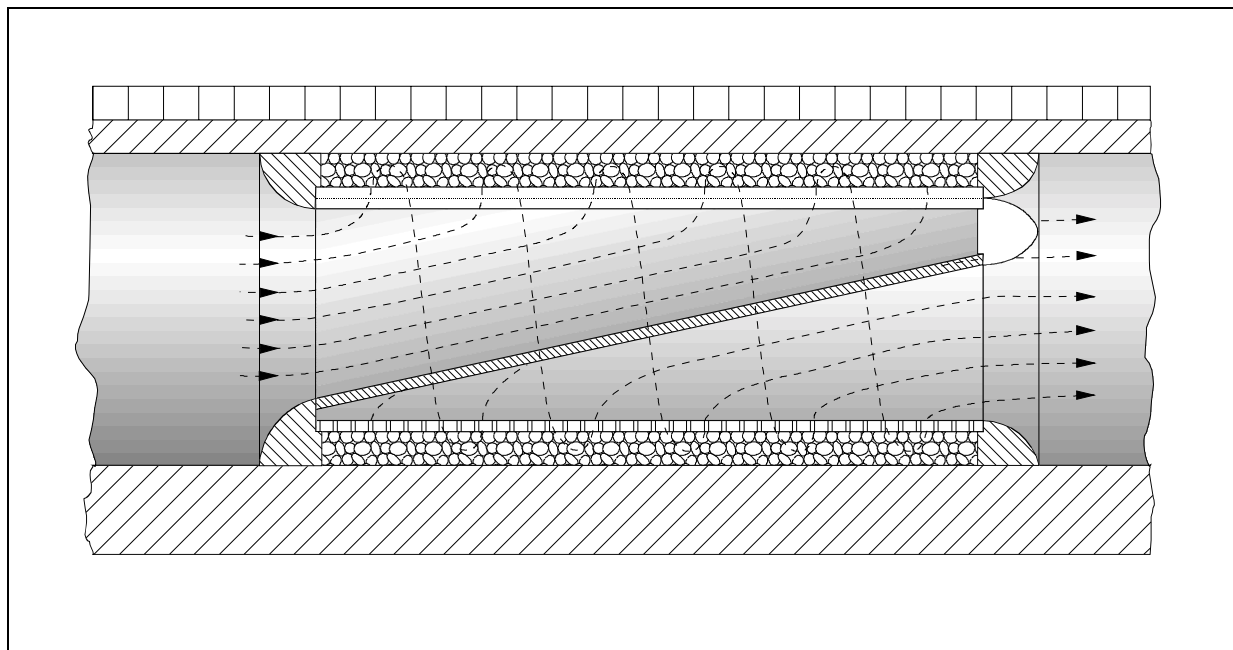


Figure 8: Longitudinal section through target plate channel (length scaled-down to 1/10)

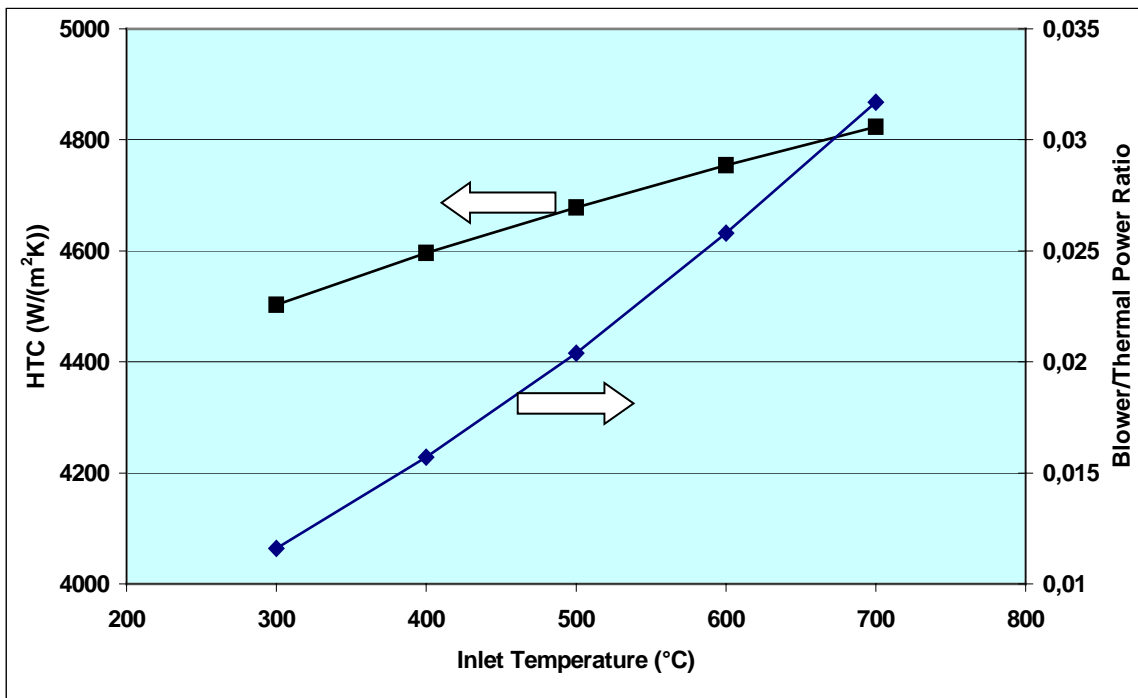


Figure 9: Heat transfer and blower power dependence from inlet temperature

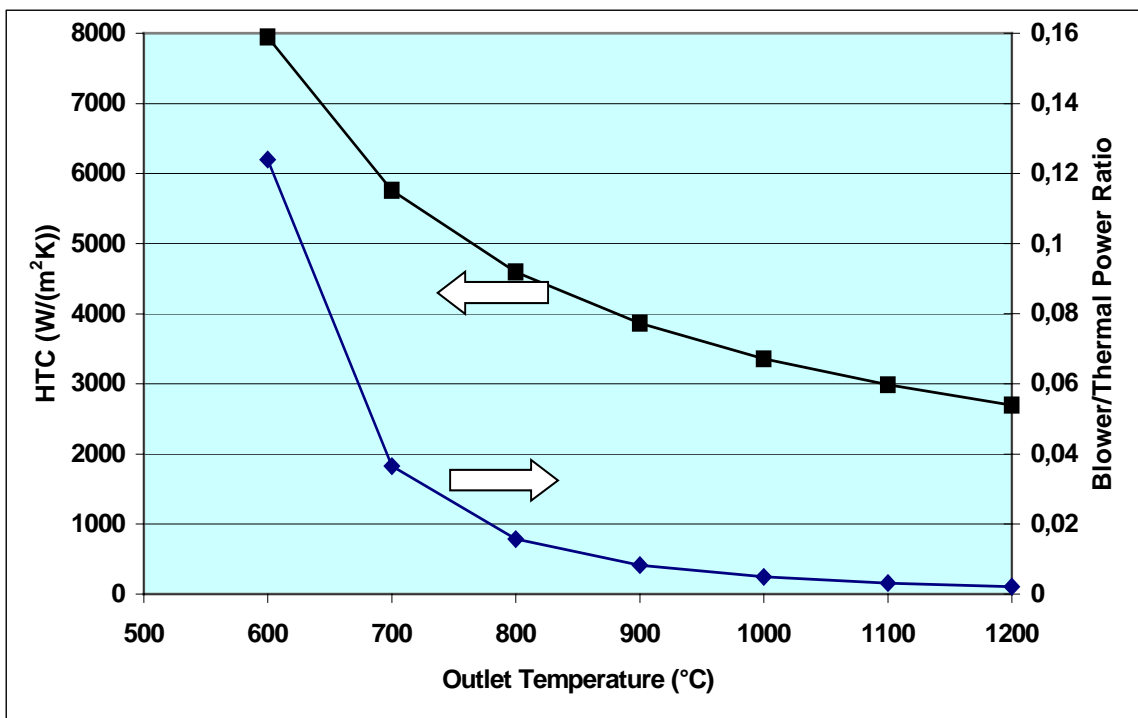


Figure 10: Heat transfer and blower power dependence from outlet temperature

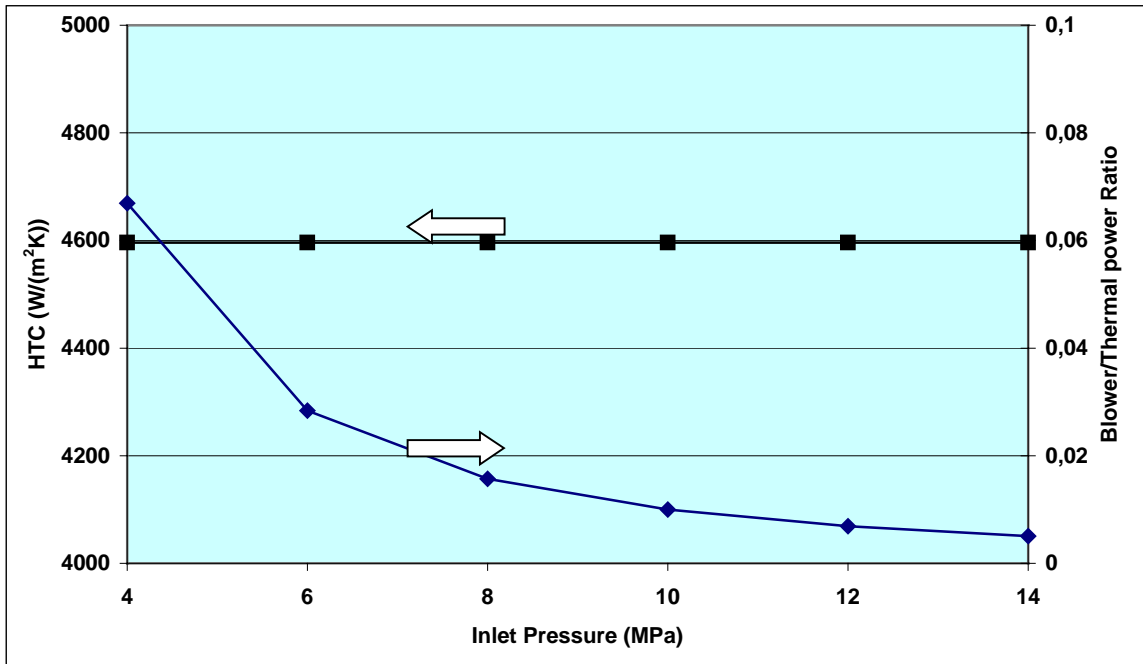


Figure 11: Heat transfer and blower power dependence from inlet pressure

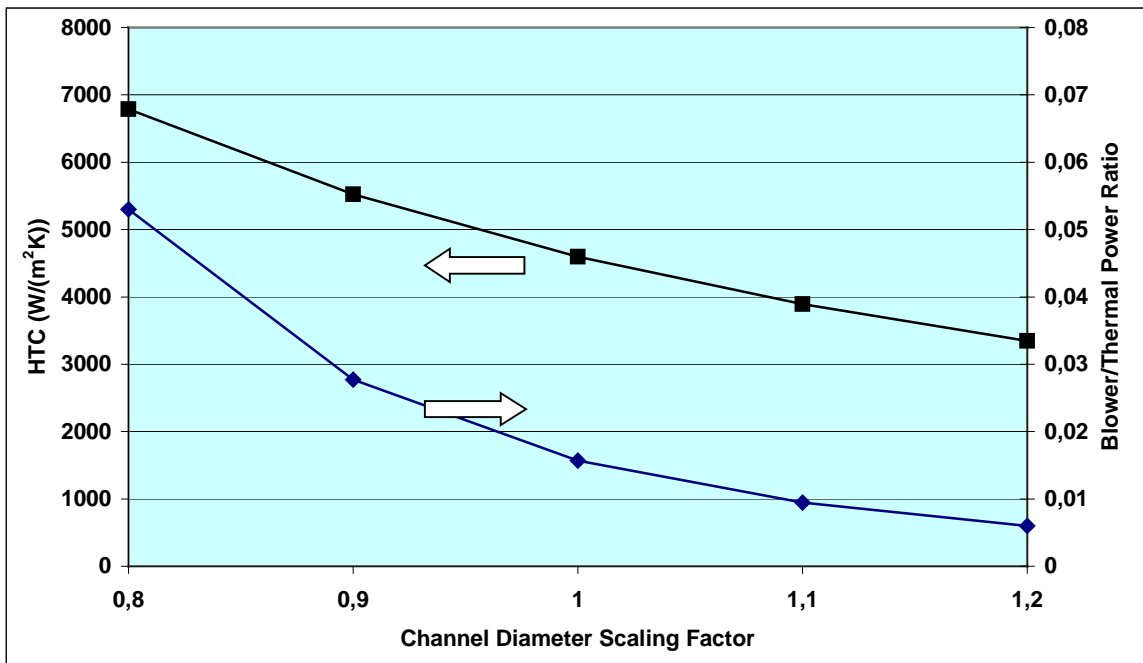


Figure 12: Heat transfer and blower power dependence from channel diameters

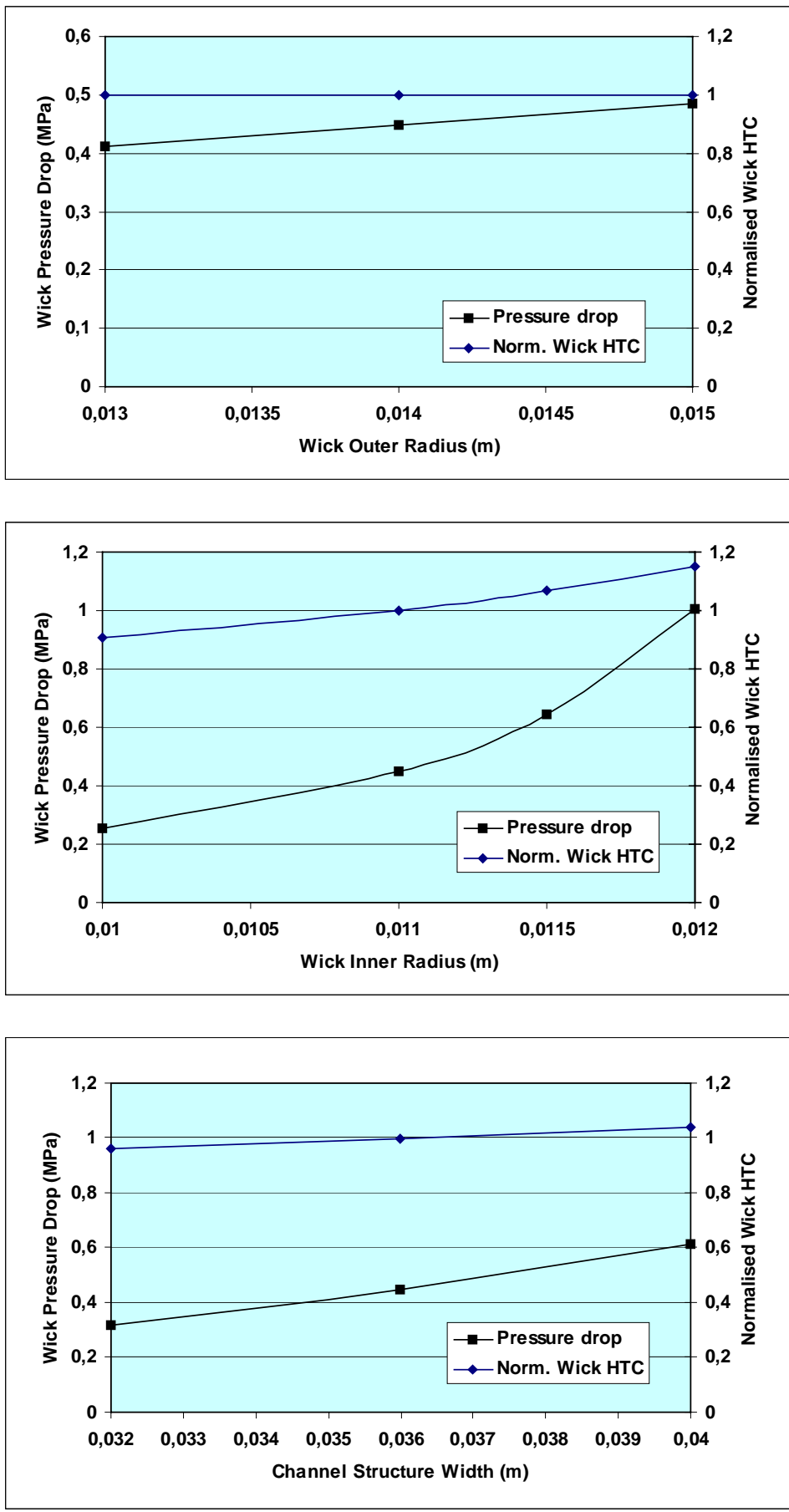
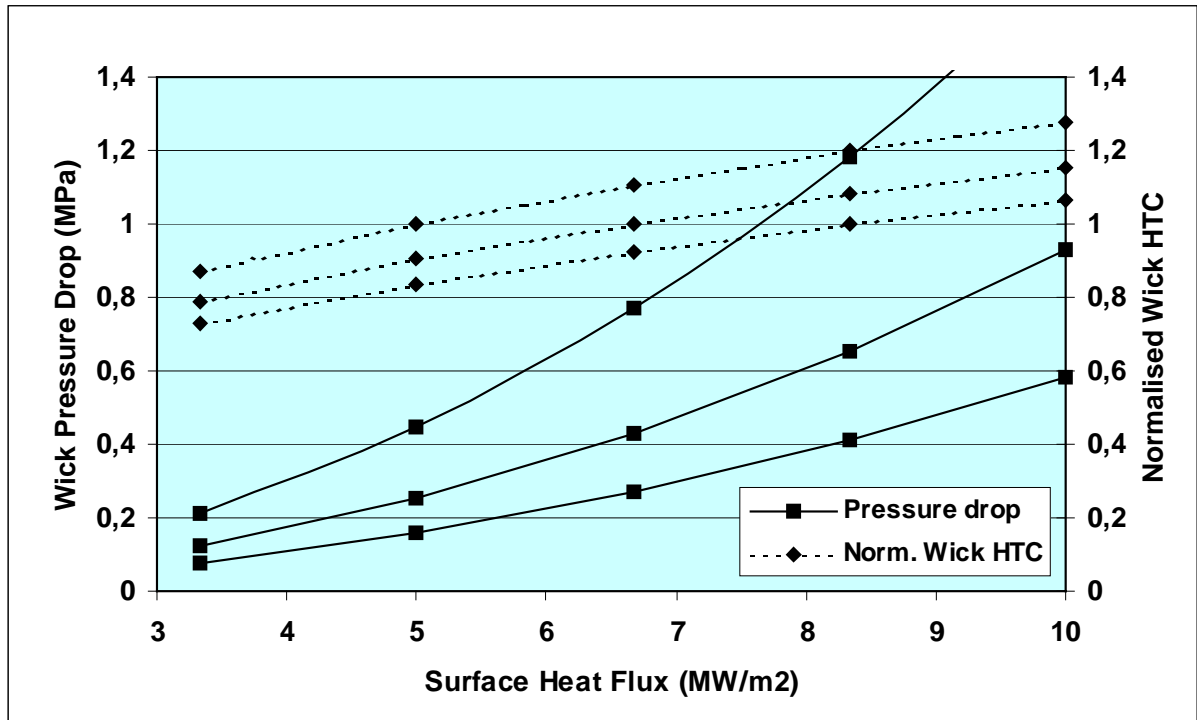
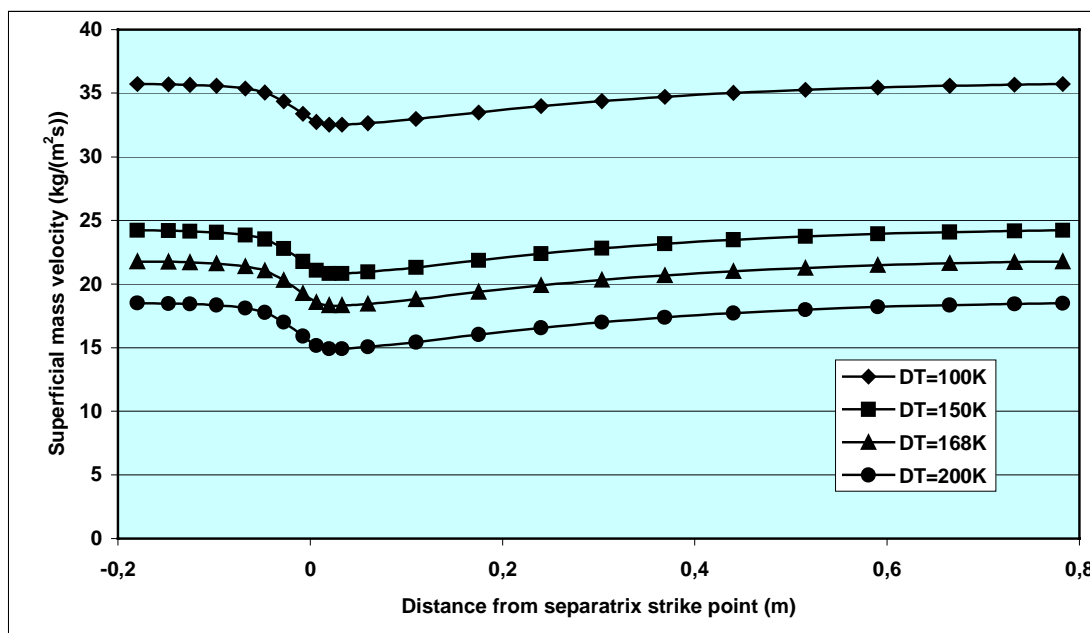
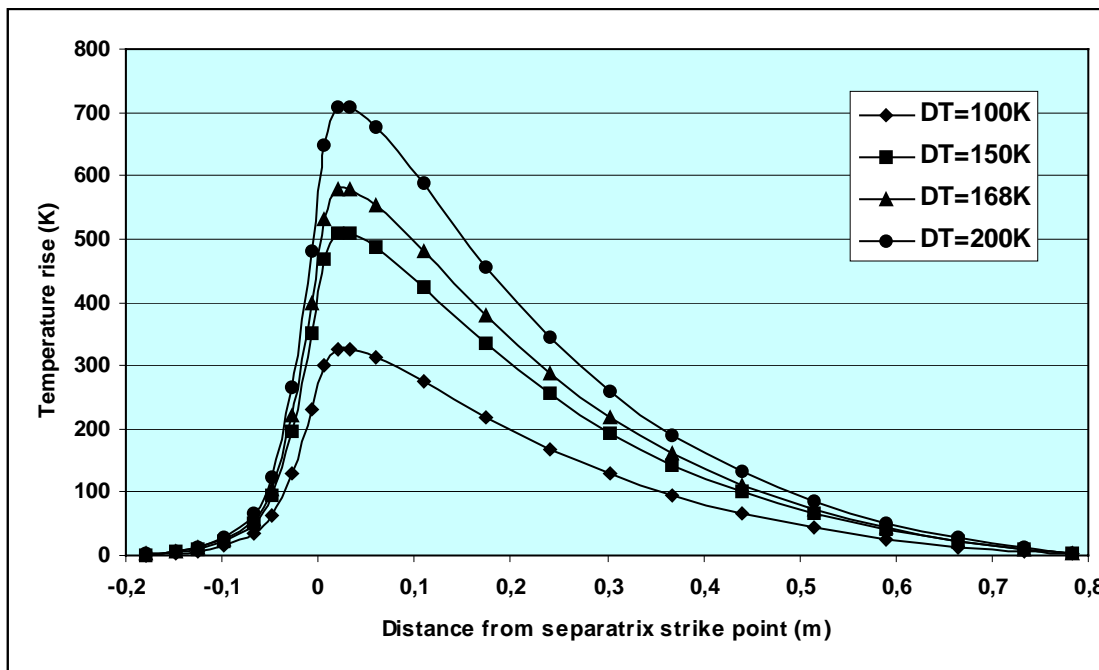


Figure 13: Dependence of pressure drop and HTC from PM geometry



**Figure 14: Dependence of pressure drop and HTC from surface heat flux**

Note: The two groups of curves represent a variation of the wick inner radius from  $r=0.011$  m (reference value, top curve in each group) to  $r=0.01$  m (centre) and  $r=0.009$  m (bottom)



**Figure 15: Axial profiles of helium temperature rise and superficial mass velocity**

**Note:** Profiles are obtained for the normalised heat flux distribution according to Figure 4 and a peak heat flux of  $9.2 \text{ MW/m}^2$ , equivalent to the assumed linear power at target plates of  $3 \text{ MW/m}$  in toroidal direction. The PM insert extends over the loaded length of 1 m. Parameter is the mean helium temperature rise, DT, with DT=168 K as the reference value.

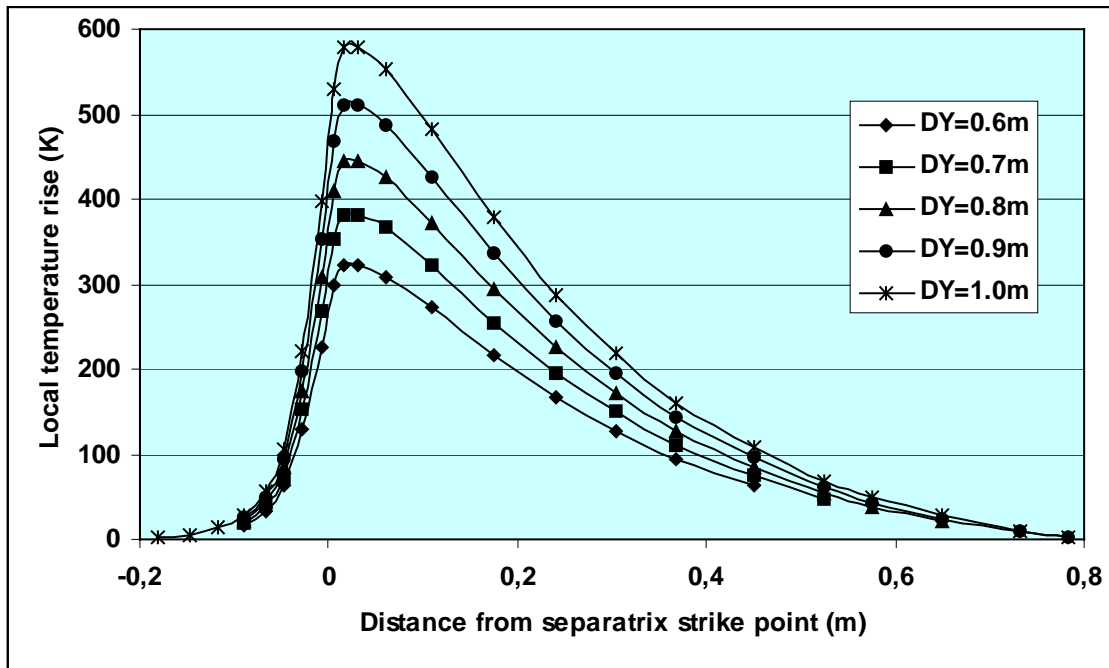
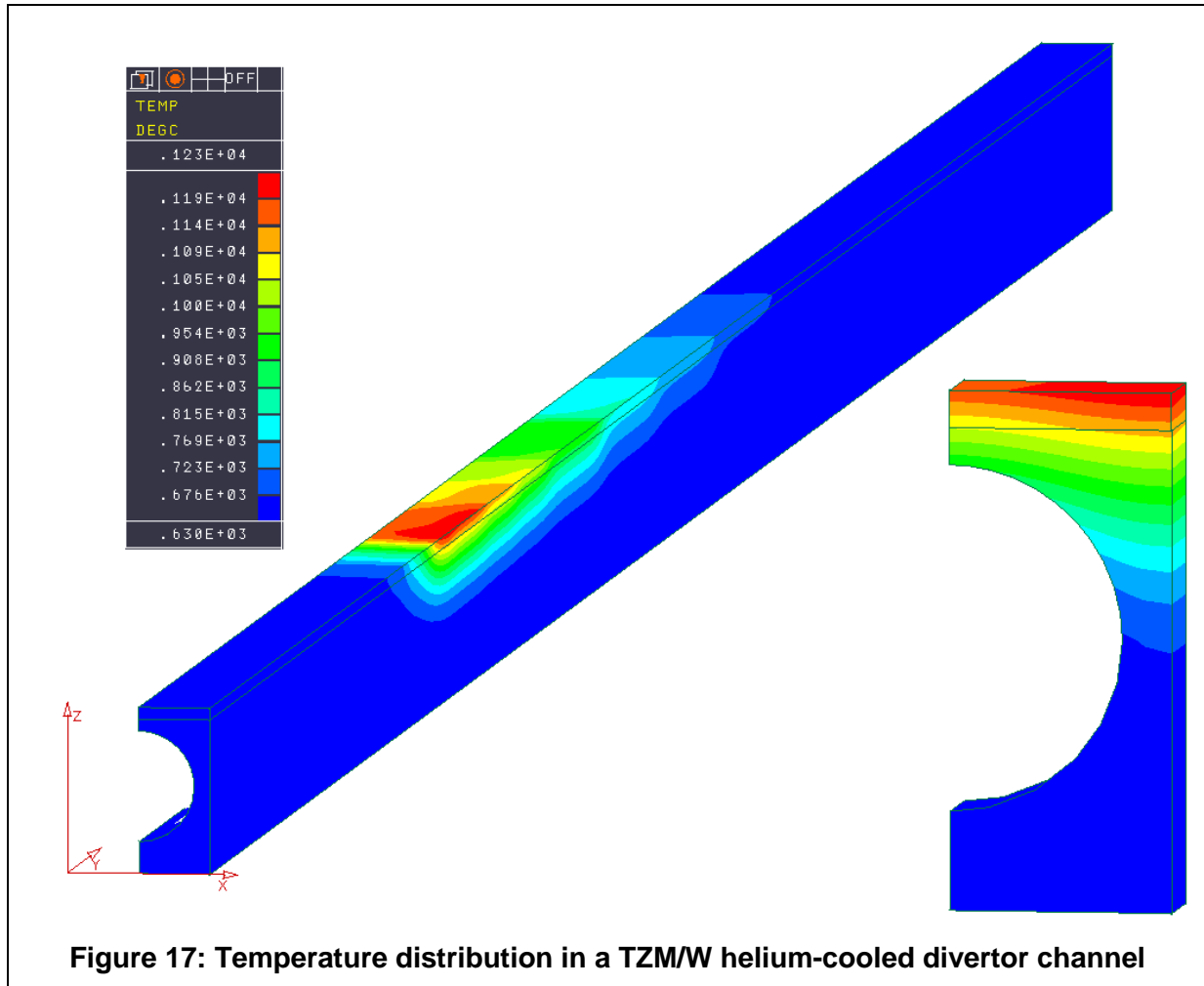
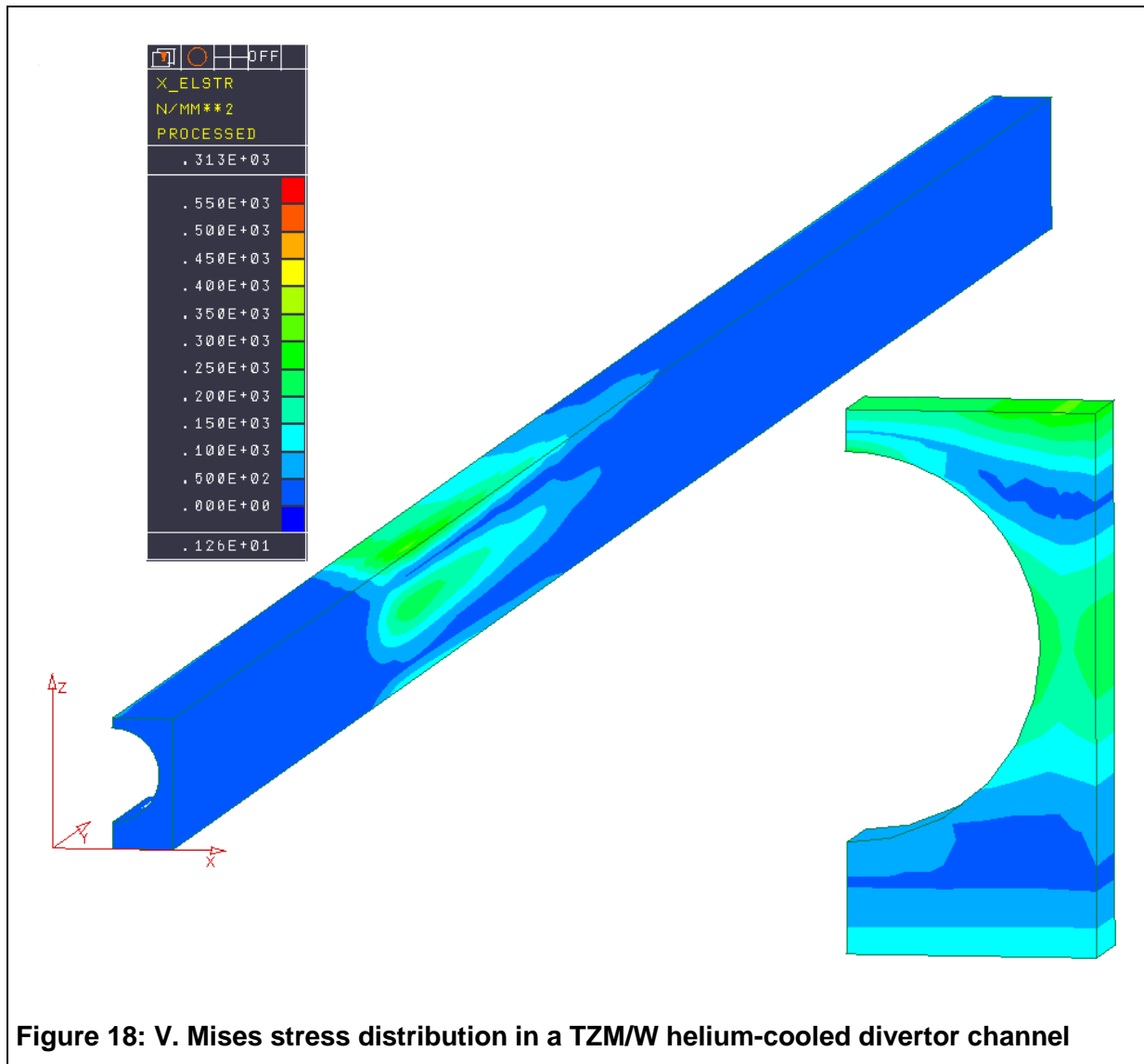


Figure 16: Axial profiles of helium temperature rise for reduced PM insert lengths



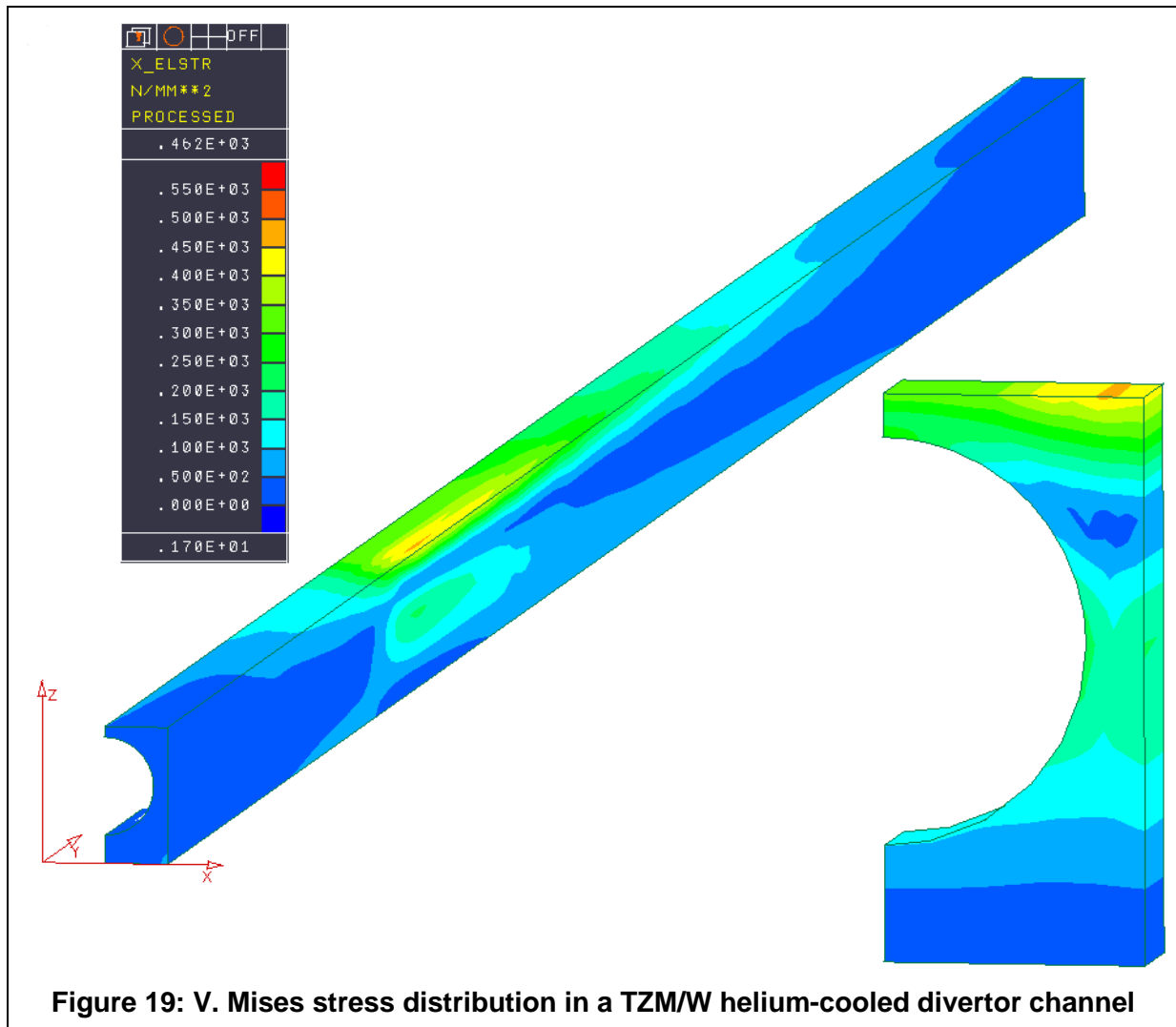


Note: Load cases 1 and 2 of thermomechanical analysis with peak heat load of 5 MW/m<sup>2</sup> (compare Table 12 on page 24).

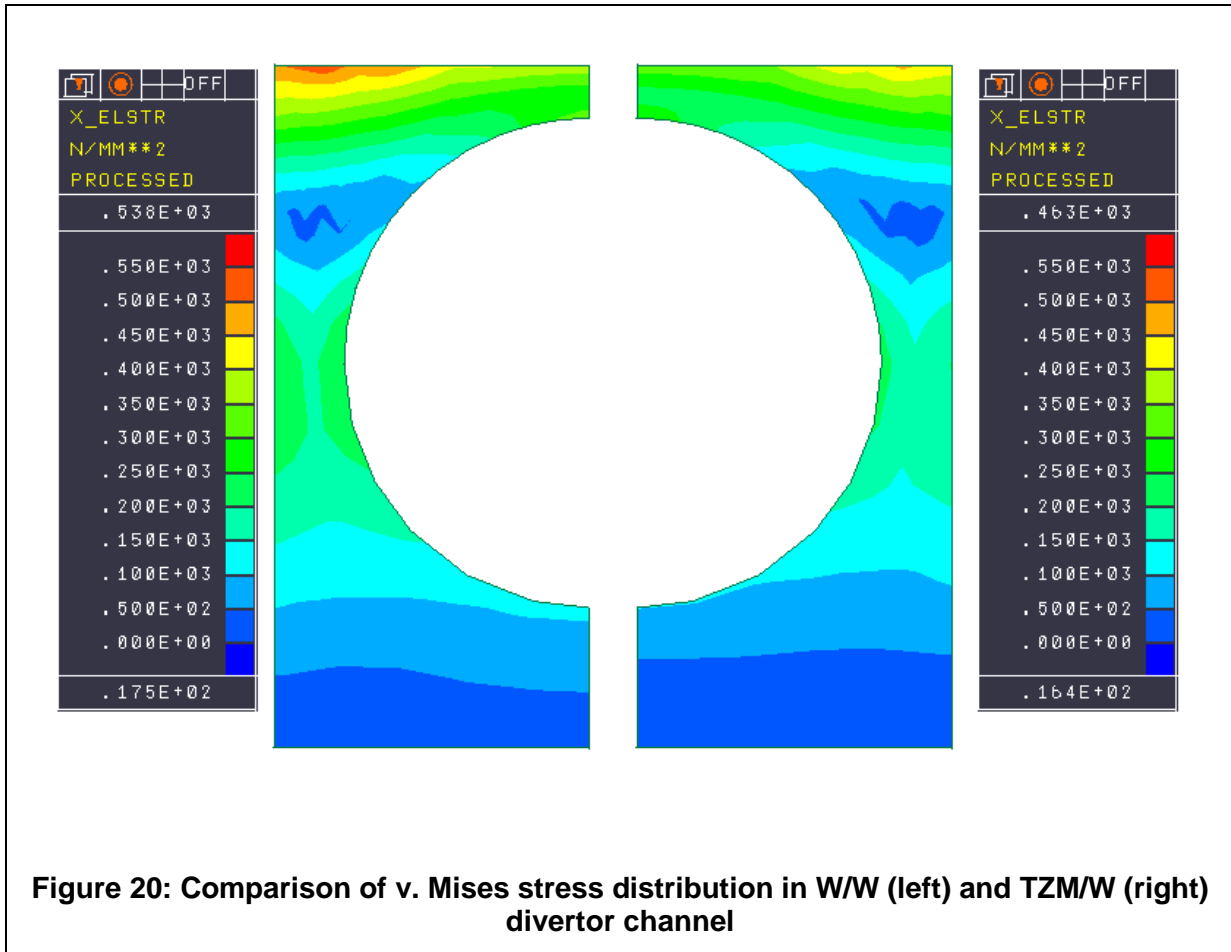


**Figure 18: V. Mises stress distribution in a TZM/W helium-cooled divertor channel**

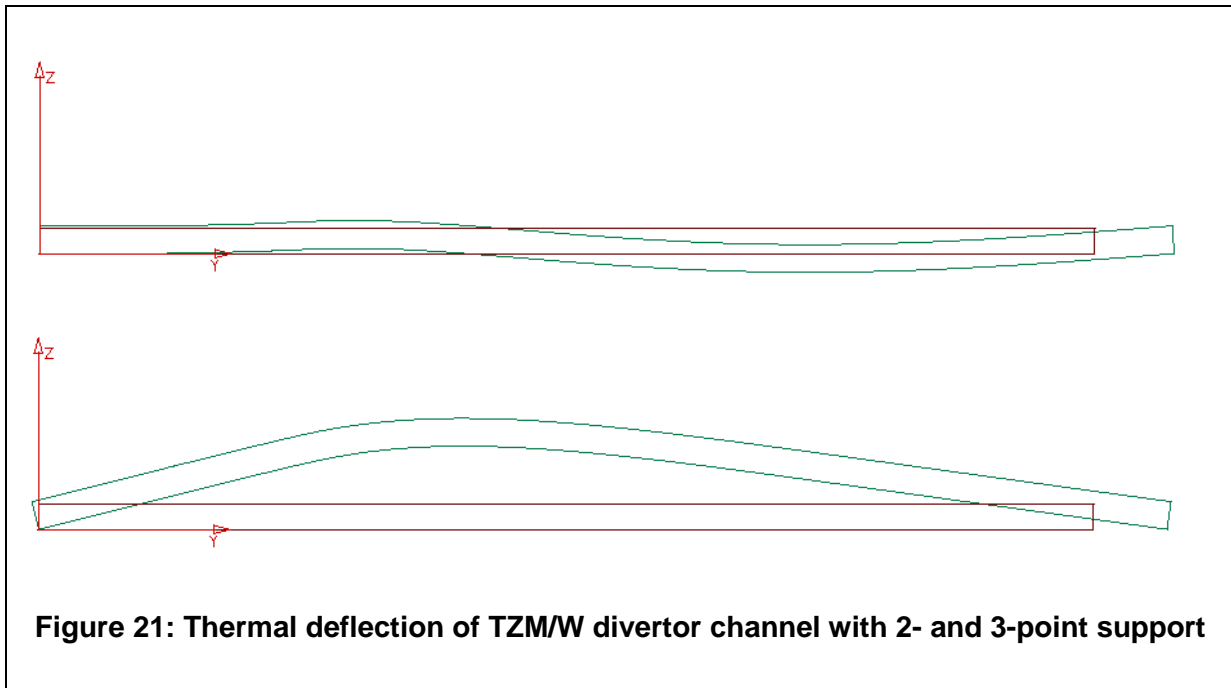
Note: Load case 1 of thermomechanical analysis with peak heat load of 5 MW/m<sup>2</sup>, 2-point support (compare Table 12 on page 24).



Note: Note: Load case 2 of thermomechanical analysis with peak heat load of  $5 \text{ MW/m}^2$ , 3-point support (compare Table 12 on page 24).



Note: Load cases 6 and 2 of thermomechanical analysis



Note: Load cases 1 (bottom) and 2 (top) of thermomechanical analysis with a peak heat flux of 5 MW/m<sup>2</sup>.

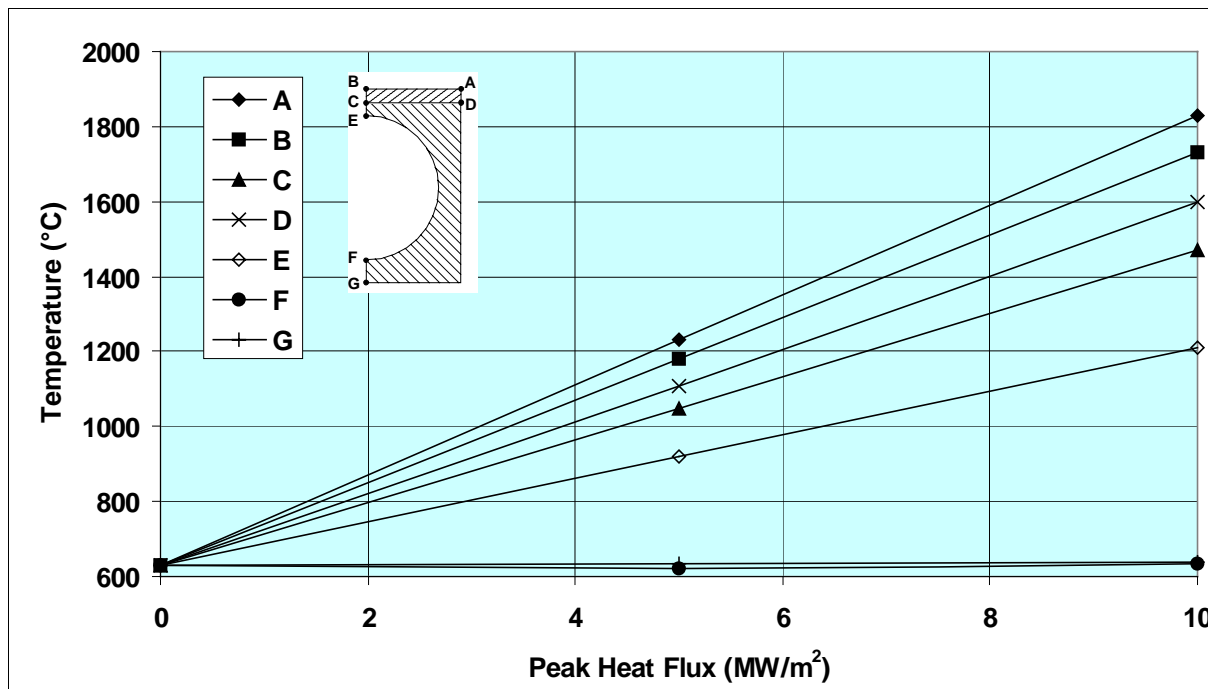


**Figure 22: Temperature at distinct points of TZM/W divertor channel vs. peak heat flux**

Note: Temperature limit of 1800 °C of W armour is reached at point A at 9.7 MW/m<sup>2</sup>.  
 Temperature limit of 1200 °C of TZM structure is reached at point D at 5.9 MW/m<sup>2</sup>.

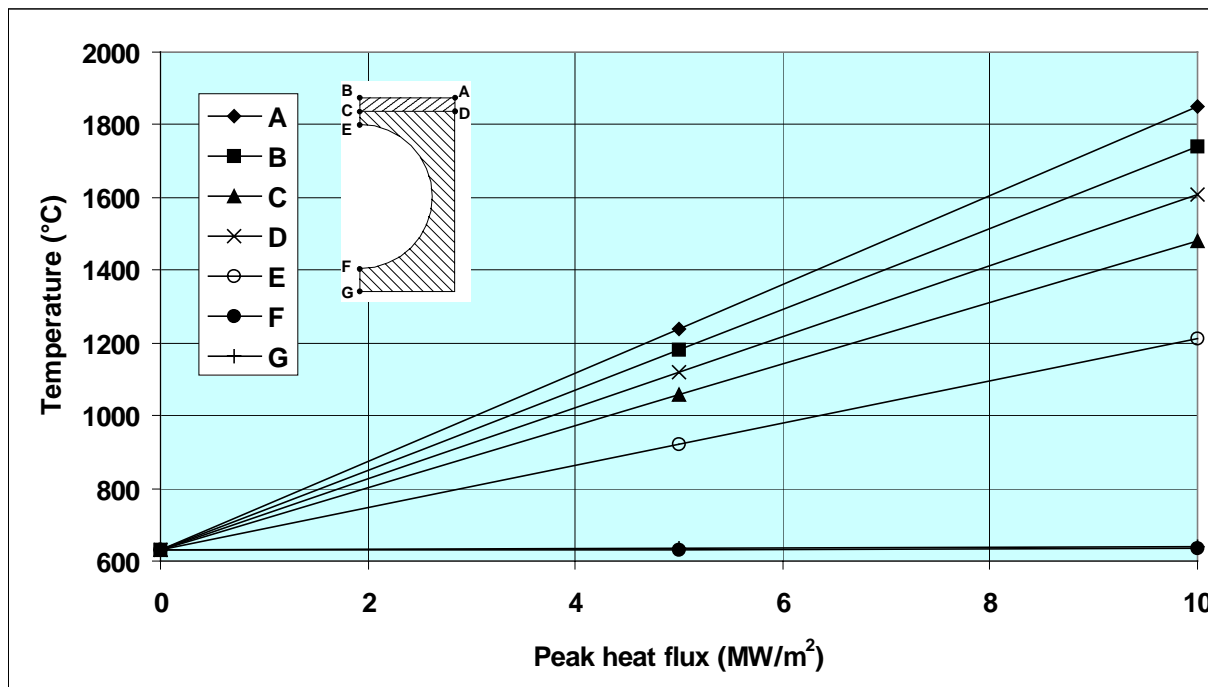


**Figure 23: Temperature at distinct points of W/W divertor channel vs. peak heat flux**

Note: Temperature limit of 1800 °C of W armour is reached at point A at 9.5 MW/m<sup>2</sup>.  
 Temperature limit of 1400 °C of W structure is reached at point D at 7.8 MW/m<sup>2</sup>.

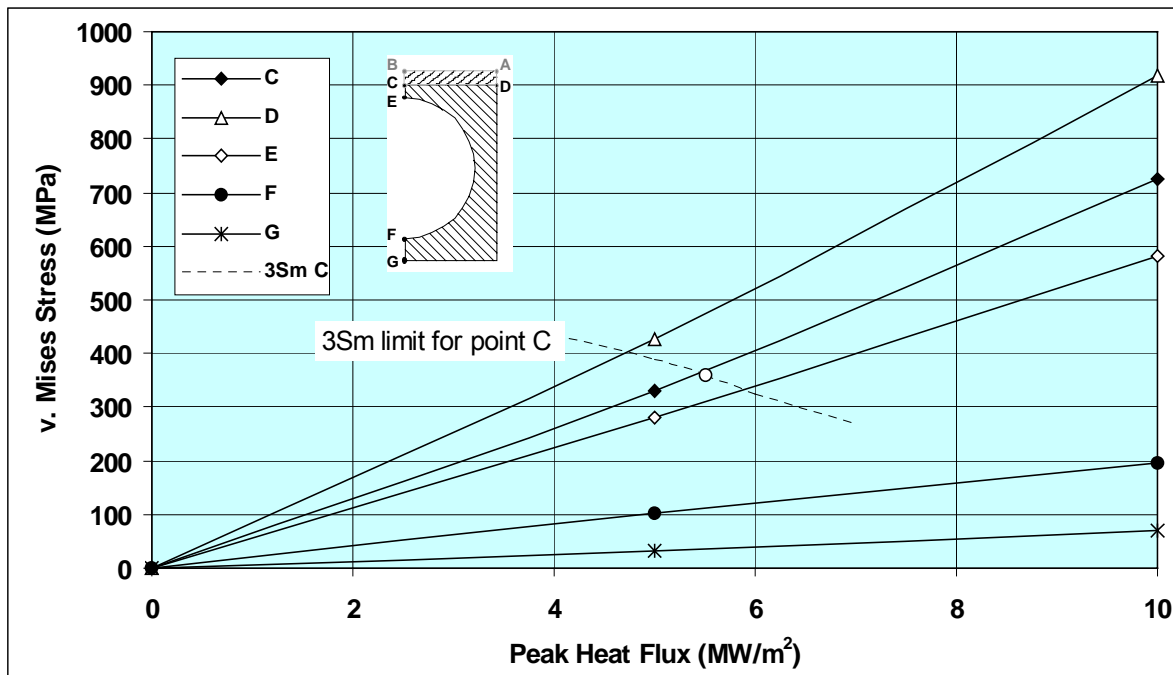


Figure 24: V. Mises stress at distinct points of TZM/W divertor channel vs. peak heat flux

Note: Curves for points C to G are obtained for 3-point support. The dashed line indicates the temperature dependent 3Sm limit pertaining to point C considered as the critical point. It intersects the stress curve of point C at a peak heat flux of 5.5 MW/m<sup>2</sup>.

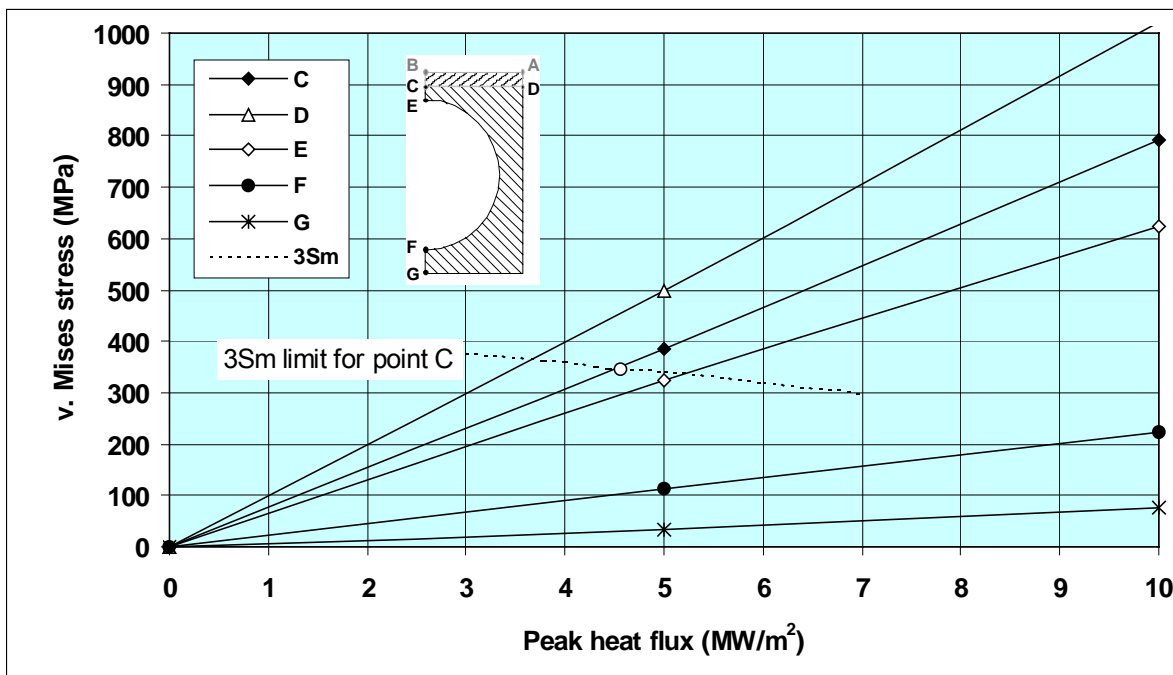
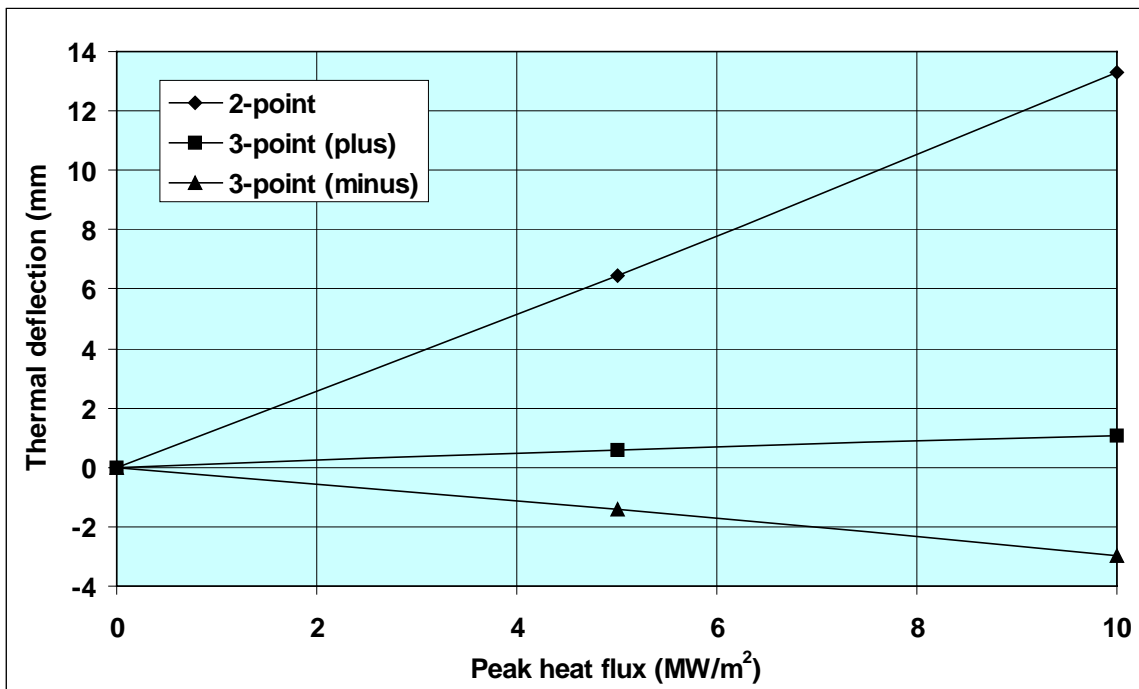


Figure 25: V. Mises stress at distinct points of W/W divertor channel vs. peak heat flux

Note: Curves for points C to G are obtained for 3-point support. The dashed line indicates the temperature dependent 3Sm limit pertaining to point C considered as the critical point. It intersects the stress curve of point C at a peak heat flux of 4.5 MW/m<sup>2</sup>.



**Figure 26: Thermal deflection of TZM/W divertor channel vs. peak heat flux**

Note: Deflections plotted are the extreme values along the channel axis obtained for load cases 1 to 4 as listed in Table 15 for 2-point and 3-point support. The 3-point support has two extremes, one at  $y=0.48$  m towards the plasma (denoted as plus) and the other at  $y=1.17$  m pointing away from the plasma (minus). See also Figure 21.

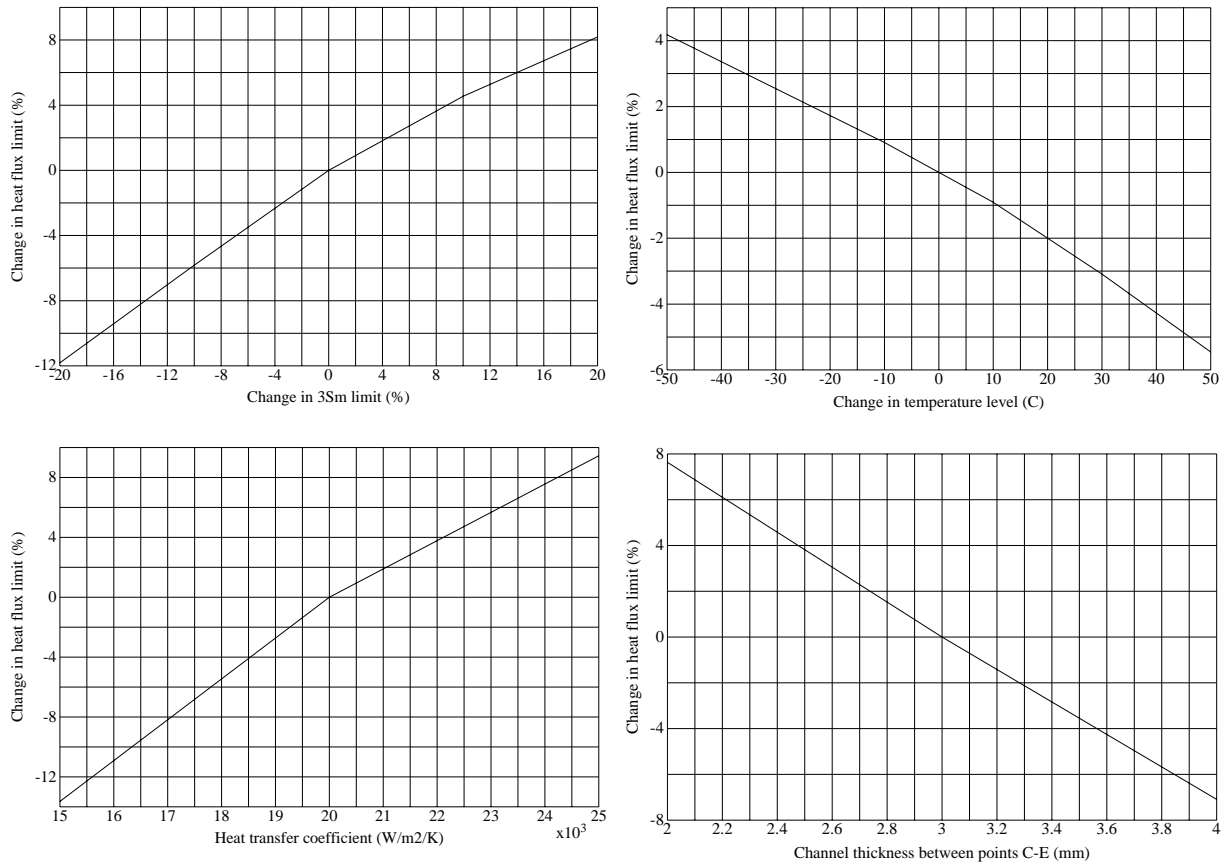


**Figure 27: Sensitivity of heat flux limit on various parameters**

Note: This sensitivity study has been performed for the TZM/W divertor channel with 3-point support as the best performing variant investigated in Chapter 3 that led to the performance limit of 5.5 MW/m<sup>2</sup> (compare text in section 4.2 on page 29). Changes in heat flux limit are plotted here relative to 5.5 MW/m<sup>2</sup>.